# Spectroscopic Analysis of the Gamma Doradus Variable HD 135825 with iSpec and ASPiS

**Edward Snowdon**

Master of Science (by research)

University of York,
Physics
September 2019

## Abstract

Determination of the atmospheric parameters and chemical abundances of $\gamma$-Dor stars is of significant importance to the ongoing efforts to study their compositions, origins and interior workings. Spectroscopic analysis of the $\gamma$-Doradus variable star HD 135825 and three spectroscopic standard stars HD 22879, HD 49933 and HD 61421 was carried out using synthetic spectral fitting methods. A suite of automation scripts, referred to as ASPiS, was created to allow streamlined analysis via use of the iSpec software package. The parameter and abundance results for the standard stars showed good agreement with literature values and confirm the validity of the ASPiS methodology. Analysis of HD 135825 revealed abundance and parameter values in line with expectation but with large fractional uncertainties, indicating further revision is needed for use of this method with $\gamma$-Dor stars. A possible link between the pulsation phase of an observation and the fitting of the surface gravity and projected equatorial velocity parameters was established from the analysis of HD 135825. This may potentially impact studies attempting to apply a single uniform parameter fit to large observational datasets taken over extended periods of time. Instead, it may be advantageous to perform analyses on smaller sets of data taken within a smaller timeframe where pulsational effects will be minimised.

# Contents

# List of Figures



# List of Tables

## Acknowledgements

The author wishes to thank Dr. Emily Brunsden for her invaluable work in guiding and supervising this project. Additional thanks are also owed to Dr. Ewa Niemczura for her consultation and advice, Dr. Sergi Bianco-Cuaresma and collaborators for their work in developing and maintaining iSpec, as well as the various personnel involved in data collection at the University of Canterbury Mt. John Observatory.

# Declaration

I declare that this thesis is a presentation of original work and that I am the sole author. This work has not previously been presented for an award at the University of York, or any other institution. All sources are acknowledged as references.

The code base developed in this project is available online at:

https://github.com/Ted-S-York/ASPiS

# 1 Introduction

Spectroscopic analysis is a principal method for the exploration of the composition and inner workings of the stars. This work aims to apply this method specifically to the Gamma Doradus ($\gamma$-Dor) classification of variable stars, with the goal of determining atmospheric parameters and chemical abundances for a range of species. This will contribute to the overall corpus of study on these stars, while also assessing the effects that the unique nature of $\gamma$-Dor variables has on the spectroscopic method. To facilitate this, a suite of automation codes, collectively referred to as ASPiS (Automated Spectrum Processing with iSpec) has been developed to allow for streamlined preparation and processing of stellar spectra using iSpec analysis software v2019.03.02 [1].

The following sections will provide the conceptual context for this work, as well as describe the current state of research into $\gamma$-Dor variables and outline the goals of this study in detail. The internal processes present in $\gamma$-Dor targets will be described with emphasis on their effects on observed spectral line profiles. The process of abundance and parameter analysis will be discussed including explanations of synthetic spectral fitting and methods of error calculation for chemical abundances. The analysis pipeline will be tested first using spectroscopic standard stars to demonstrate the validity of the method, and then applied to the known $\gamma$-Dor star HD 135825.

## 1.1 A Brief Introduction to Spectroscopic Astronomy

Since Isaac Newton first demonstrated how white light may be divided into a spectrum of its component parts, spectroscopy has developed into a critical tool for studying and understanding of the nature of stars and other astronomical objects. The use of spectroscopy in astronomy was pioneered by Fraunhofer who used the observation of absorption lines to identify the presence of chemical elements in the Sun (1814) and other bright stars (1817) [2]. Further advances included early attempts to photograph stellar spectra by Huggins and Miller (1864) and the development of the objective prism spectrograph by Draper (1879) which allowed for the study of stars too faint to be visible to the naked eye [2]. By the time of the invention of the coudé spectrograph by Adams in 1911, combined advances in spectrograph, telescope and camera technology were allowing astronomers to achieve resolving powers 30 to 100 times greater than Fraunhofer had used a century earlier [2].

The basic form of an astronomical spectrograph has undergone refinements and improvements over time but the core design principles have largely stayed the same. An entrance slit is placed at the focus of a telescope, with a collimating lens directing the divergent beam onto a dispersing element (either a prism or grating) and then into a camera that focuses the dispersed light onto a detector [2][3]. To ensure high-quality measurements, the instrument can be mounted at the coudé focus of a telescope to ensure stable alignment and minimal thermal and gravitational flexure, or alternatively a fibre-fed instrument may be used [3].

Compared to other methods, such as photometry, studies of spectral lines require a very high resolution to achieve good results. Depending on the width and structure of the lines being measured, $\lambda/\Delta\lambda$ ratios of 100 000 and above are not uncommon [3]. This necessitates a small wavelength interval per detector pixel, around 15-20 mÅ. This contrasts starkly with wide-band photometry, which may use intervals as large as 1000 Å[3]. High-resolution spectroscopy is most effective when studying bright stars; as a practical

example, a 30 minute exposure of a 6th magnitude star can be realistically expected to yield a signal-noise ratio of around 100 using a 1 m aperture telescope at a resolving power of greater than 100 000 [3].

Spectral features contain a great deal of information about an observational target. Since the resting wavelengths of atomic transitions are very well known, spectral lines can be used to measure the motion of objects to a high precision, this has led to significant discoveries such as the Hubble flow, galactic rotation curves and the kinematics of binary stars [4]. The degree of excitation of a star's spectrum, as measured by the relative strengths of lines, is used to determine stellar spectral classifications [4]. The strengths and numbers of lines is also key to determining the chemical composition and abundances within target objects, such data have been crucial in the development of nucleosynthesis models and the understanding of the formation and evolution of different stellar populations [4].

## 1.2 Gamma Doradus Variable Stars

Gamma Doradus ($\gamma$-Dor) variables are a classification of variable star characterised by high radial order, low angular degree g-mode pulsations of approximately 0.1 magnitudes over periods of the order of one day [5]. $\gamma$-Dors are typically young, late-A to early-F type main-sequence stars [5] with metallicities generally at or below Solar levels [6]. The long durations of $\gamma$-Dor pulsations make ground-based observation challenging, and thus much of the study of these stars has taken place over long periods of time, between several observation sites, or using space-based instruments.

Variability in $\gamma$-Doradus, the eponymous star of the class, was discovered by Cousins & Warren (1963) to manifest in changes of several hundredths of a magnitude with two primary periods of 0.757 and 0.733 days [7]. $\gamma$-Doradus is of a similar brightness to that expected of a $\delta$-Scuti star but has a lower temperature and much longer pulsation periods. For some time this led to $\gamma$-Doradus being regarded as an anomaly; starspots were proposed as a possible explanation but the length and stability of the variabilities, coupled with the discovery of a third periodicity in 1996 resulted in the abandonment of this hypothesis [8]. Krisciunas et al. (1993) discovered similar long-period variability in the star 9-Aurigae, finding two photometric periods of 1.2 and 3 days [8]. During the 1990s, analogous pulsations in several more stars were discovered, eventually leading to the classification of $\gamma$-Dor stars as a distinct family of variable stars [6][8].

On the Hertzsprung-Russell (H-R) diagram, $\gamma$-Dors are found on the cool edge of the instability strip [5]. There is therefore a degree of overlap between $\gamma$-Dor and $\delta$-Scuti stars in this region, with stars potentially exhibiting both $\gamma$-Dor (high-order, long, g-mode) and $\delta$-Sct (low-order, short, g- and p-mode) pulsations [9]. Frequency analysis of the quarter 0 and 1 data from the *Kepler* mission, taken from a large sample of variable stars within the instability strip showed that practically all the stars surveyed displayed frequencies in both the $\gamma$-Dor and $\delta$-Sct ranges [9]. As a consequence, modern studies now approach these variable stars by considering the component frequencies and thereby classifying them into $\gamma$-Dor, $\delta$-Sct or hybrid based on the dominant region in which pulsations occur [9].

Variability in $\gamma$-Dor stars is understood to be driven by a process of convective blocking in the stellar interior [10]. These stars possess convective cores and shallow convective envelopes, separated by a radiative transfer zone [11]. During pulsation, convective processes can not adapt to transport the additional luminosity produced; this results in a

'blocking' of luminosity at the base of the convective zone, resulting in pulsation driving [10]. The convective blocking mechanism was first proposed by Cox et al. (1987 & 1993) to describe pulsations in white dwarfs [12][13], but was deemed not to be viable as the convective timescales in the thin convective zones of white dwarfs are significantly shorter than the pulsation period [10]. Guzik et al. (2000) successfully applied convective blocking to reproduce $\gamma$-Dor g-modes with periods of 0.4 to 3 days, consistent with observation [10]. Due to the nature and location of the blocking mechanism, it can coexist with the driving mechanism of $\delta$-Sct pulsation, namely the $\kappa$ mechanism within the He II ionisation zone [9]. This coexistence is what allows the very high degree of hybridisation between the two classifications to exist.

The study of variable stars is of significant importance to stellar physics in general and asteroseismology in particular. The study of stellar pulsations is a powerful tool for probing the interior structure of stars, and since pulsation occurs in a wide variety of stars and varies over time, it is of great importance to the understanding of stellar evolution [11]. The specific study of $\gamma$-Dor stars is a frontier in the investigation into the formation, structure and evolution of intermediate-mass stars [6]. The use of $\gamma$-Dors as analogues has also been employed in the successful search for solar g-mode pulsations [8].

## 1.3 iSpec

Since the origins of computational spectroscopy, a wide range of analysis codes have been developed that have been used in various combinations by different researchers [14]. However, the intrinsic differences in the disparate codebases can result in compatibility issues that require complex systematic solutions that increase the difficulty of spectroscopic analysis [14]. iSpec is a Python-based software package developed by Sergi Blanco-Cuaresma and collaborators that aims to improve the analysis procedure by gathering together a range of popular code options within a mutually-compatible framework, with the main goal being to facilitate easy analysis of atmospheric parameters and chemical abundances [1].

Various model atmospheres, radiative transfer codes, solar abundances and reference linelists are provided with iSpec and can be easily selected by the user. This allows for simple tailoring of the code to work with spectra from any star in the A-M spectral range to reasonable accuracy [14]. Several spectral preparation processes, such as the removal of telluric lines, are available and the analysis of atmospheric parameters and chemical abundances can be carried out using either Synthetic Spectral Fitting or the Equivalent Width Method [1]. As a Python-driven package, iSpec can be readily modified by the user. This can include the addition of non-standard linelists or models, the creation of custom functions and the automation of processes via scripting. By default, iSpec is controlled through an accessible GUI but it is also possible to run in a terminal, particularly if using scripting.

## 1.4 State of Current Research

Research on the subject of variable stars, with respect to $\gamma$-Dors in particular, has been significantly galvanised in recent years following the release of data from the *Kepler* mission. Prior to *Kepler*, there were approximately 100 stars known to exhibit $\gamma$-Dor variability [6]. Following the mission data releases, more than 2000 candidate $\gamma$-Dor, $\delta$-Sct or hybrid stars have been identified [15] and as of 2016, the Variable Stars Index listed

approximately 400 identified $\gamma$-Dors [16].

Detailed studies of individual variable stars are often focused on determining atmospheric parameters, chemical abundances and pulsation frequencies. Kahraman Aliçavuş et al. (2015) studied 52 targets using 5 separate instruments located in Spain, Chile and New Zealand [6]. Atmospheric parameters were derived from analysis of Hydrogen and Iron spectral lines using ATLAS9 and SYNTHE atmospheric modelling and spectral synthesis codes. Spectral classifications were determined using Balmer lines, Fe/Ca/Mg metal lines and Ca II k-line/G-band lines, the use of all three methods gives reliable classification while also identifying chemically-peculiar targets such as Am stars. The $\gamma$-Dor targets in the sample were found to have a range of effective temperatures from 7100 to 7300 K, log(g) values of 3.8 to 4.5 dex, a wide $v\sin i$ range of 5 to 240 $\mathrm{kms}^{-1}$ and microturbulence velocities of 1.3 to 3.2 $\mathrm{kms}^{-1}$, peaking between 7000 and 8000 K. No correlation was found between atmospheric parameters and abundances, but strong correlations were found between the abundance of Iron and that of several other elements including Mg, Si, Ca, Sc, Ti, Cr, Ni, Y and Ba. Chemical abundances for both candidate and bona fide $\gamma$-Dors were measured to be at or slightly below Solar values, with no significant distinction between bona fide and candidate stars. It was found that there was no clear delineation between the edges of the $\gamma$-Dor and $\delta$-Sct instability strips, and high numbers of hybrid stars were detected in both regions.

Significant work has been performed focusing on comparisons and correlations between the properties of $\gamma$-Dor and $\delta$-Sct stars. Qian et al. (2018) analysed LAMOST data for 168 $\gamma$-Dor stars and investigated their relationship to long-period ($> 0.3$ d) $\delta$-Sct variables [16]. They found their sample to have early-F spectral types, a temperature range of 6880 to 7280 K and average metallicities of 0.4 to 0. They note that some $\gamma$-Dor and $\delta$-Sct stars lie beyond the borders of the region on the H-R diagram predicted by current theories. They also discovered similarities between the physical properties of long-period $\delta$-Sct stars and $\gamma$-Dors, for instance the atmospheric parameters of short-period $\delta$-Scts are correlated with pulsation period, while no similar relation exists in either long-period $\delta$-Scts or $\gamma$-Dors.

The internal processes within $\gamma$-Dor stars are of particular importance to spectroscopic studies due to the knock-on effects on line profiles. Van Reeth et al. (2015) note that the mechanics of rotation and chemical mixing within stellar interiors are largely unknown, this is a key element in the evolution of the convective cores of intermediate mass stars (between 1 and 2 solar masses) [17]. Asteroseismic study of $\gamma$-Dor is a useful tool for calibrating and improving upon evolutionary and structural models within this range. They noted a strong correlation between $v\sin i$ and period spacing values, suggesting a quantifiable influence of rotation on pulsation characteristics. They also found relations between rotation, temperature, dominant g-mode frequencies and the longest period of pulsation [17]. Aerts, Mathis & Rogers (2019) explain that the mixing profile in medium- to high-mass stars are affected by several processes including convective overshooting and rotationally-induced angular momentum transport [18]. Overshooting in the specific context of $\gamma$-Dor stars was studied by Lovekin & Guzik (2017) by investigating its effects on the pulsation properties of a grid of stellar models between 1.2 and 2.2 $M_{\odot}$ [19]. They found that by calculating the pulsation constant for all models in the grid, constraints can be placed on the convective overshoot and rotation of stars. Ouazzani et al (2018) applied angular momentum transport models to $\gamma$-Dor stars and found that while some mechanism is responsible for braking of the core rotation, it cannot be explained by current transport models [20].

In order for the pulsations of $\gamma$-Dor stars to be considered, the frequency modes of the pulsations must first be identified. Brunsden et al. (2012) made use of 291 high-resolution spectra to perform mode identification of frequencies within a single $\gamma$-Dor variable HD 135825 [11]. Four frequencies were identified within a range of 0.3 to 1.9 $d^-1$ to good precision. Additionally, several other frequencies were detected but these lay below the SNR limit of the Fourier spectrum and so were not analysed further. Fitting the frequency modes to existing line profiles for HD 135825 allowed for confirmation of the star as a bona fide $\gamma$-Dor variable. It also allowed for the determination of the axial inclination and rotational velocity of the star. The requirement for such a large number of high-resolution spectra also demonstrates that detailed spectroscopy of typical $\gamma$-Dors can be very data-intensive. As observational asteroseismology begins to focus less on classification and more on identification, larger data sets will be needed.

## 1.5 Objectives of This Work

The foremost goal of this work is to successfully obtain the atmospheric parameters and chemical abundances of a the $\gamma$-Dor star HD 135825 via spectroscopic means. By accomplishing this, it is hoped to both add to the overall body of knowledge in the field as well as to create a user-friendly and simple to use analysis pipeline for future work. Spectral data will be taken from several years' worth of observation with the HERCULES spectrograph located at Mt. John Observatory, New Zealand. This spectral data will be both analysed as a whole and also separated according to the pulsational phase of each observation. This will allow for comparison between different pulsational phases of HD 135825 and between phase-separated spectra and 'averaged' overall spectra. HD 135825 was chosen due to its status as a bona-fide $\gamma$-Dor variable and its pulsation profile, which is dominated by a single mode with period 1.315 days. For validation and testing of the method, observational spectra of spectroscopic standard stars will also be taken from HERCULES. The standard stars have been selected to have moderate parameter values and a large body of published literature against which results can be compared. Data is reduced using the MEGARA pipeline and then analysed using iSpec software [1][14]. To assist with this task, a suite of automation scripts for use with iSpec will be produced to streamline and simplify the workload without compromising quality of results. These scripts are intended to be made publicly available for use in other projects.

The work should fit within the broader corpus of work on spectroscopic analysis of variable stars by providing good-quality results and novel methods. The targets to be studied have been drawn from other surveys, particularly Kahraman-Aliçavuş et al. (2015) [6] and so this will be used as a benchmark for comparison of the results of this methodology. The novel aspects presented here will be the improved analysis methods, the effects of the consideration of pulsation phase when constructing and analysing spectra and the comparison to 'average' spectra produced from continuous observations across one or multiple periods.

# 2 Theory

## 2.1 Spectral Line Formation

Discrete emission or absorption lines observed on the continuum of a star's spectrum arise from transitions between bound states of atoms in the stellar atmosphere [21]. These lines are characterised by their distributions of energy as a function of frequency, referred to as the 'profile'. With the exception of the Sun, only the integrated flux over the entire stellar disc can be observed for a given star. The line profile can then be written in terms of the absorption depth $A_\nu$, which is related to the flux in the line $F_\nu$ and in the continuum $F_c$ [21]:

$$A_\nu \equiv 1 - \frac{F_\nu}{F_c} \tag{1}$$

It is often not possible to measure a spectrum in sufficient detail to determine the line profile due to resolution limitations. In this case the profile maybe substituted by an integrated line strength referred to as the 'equivalent width' $W_\nu$. This may be defined in terms of either frequency or wavelength [21]:

$$W_\nu \equiv \int_0^\infty A_\nu \, d\nu \tag{2}$$

Or

$$W_\lambda \equiv \int_0^\infty A_\nu \, d\lambda \tag{3}$$

The equivalent width represents the width of a zero-flux line with the same area under the profile as the actual line being studied [21]. It is preferable to study line profiles rather than equivalent widths, where available, as multiple line profiles can be fitted to the same equivalent width. Interpolation based on equivalent width alone can therefore be potentially misleading.

Spectral lines may be broadened by a number of mechanisms. The presence of local velocity fields causes broadening in all spectral lines, to the extent that thermal widths are often only a fraction of the observed width [3]. Velocity fields cause a characteristic broadening that is proportional to the line wavelength, consistent with the Doppler effect [3]. Such velocity fields may be induced by the rotational or pulsational characteristics of a star, thermal motion in the stellar atmosphere, or other factors [3]. Collisional broadening occurs due to the interactions between radiating particles and their nearby neighbours [21]. This can be modelled either by approximating the interaction as an instantaneous collision that induces a sudden transition or phase shift in the radiating wavetrain [21]. Alternatively, the neighbouring particles may be considered to be a collection of perturbing bodies, giving rise to a field that fluctuates about some statistical mean value that will cause a shift in the wavetrain [21]. There is an additional 'natural broadening' caused by uncertainty in atomic energy levels, the transition between two states therefore produces a distribution of energies rather than a single, defined value [22]. Finally, miscellaneous turbulent processes in the stellar atmosphere can also cause broadening. This effect is not firmly defined but can include internal motions within interstellar clouds, or non-physical effects such as unrecognised or overlapping spectral lines [23]. In the absence of a clear physical model, a gaussian line-of-sight turbulent velocity distribution is assumed to account for these effects [23]. The root-mean-square value of this distribution is commonly

referred to as the 'microturbulence velocity' or $v_{mic}$, and represents processes operating on length scales smaller than the photon mean free path. Processes on longer length scales will affect the observed line profile, but not the absorption profile, and may be characterised by the 'macroturbulence velocity' or $v_{mac}$ [23].

## 2.2 Effects of Pulsation on Line Profiles

The pulsational characteristics of a star can have a profound impact on the light observed, and thus affect spectral-line profiles. As a result, observation of Line Profile Variations (LPVs) is a common diagnostic technique for identification of oscillatory modes in pulsating stars [24]. Both high- and low-resolution investigations of pulsating stars have determined that there is a great diversity of pulsational amplitude and phase variations in different wavelength regions, including between individual spectral lines [25].

In asteroseismology, stellar pulsation modes are classified using the quantum numbers $n$, $l$ and $m$ [26]. The radial order, namely the number of radial nodal shells, is represented by $n$. $l$ represents the angular degree, or the number of nodal lines on the stellar surface. Modes which have $l = 0$ are referred to as 'radial', while modes with a higher degree are referred to as 'nonradial'. $m$ represents the azimuthal number, or the number of nodal lines crossing the stellar equator. The azimuthal number normally does not affect the mode frequency unless there is some symmetry-breaking effect, for instance if the star is rotating [27]. The g-mode pulsations of $\gamma$-Dor stars are of high radial order and low angular degree, and have significant rotational velocities [5].

Pulsational displacement of the stellar atmosphere creates a velocity field on the visible surface of a star. For a given point on this surface, this will induce a local Doppler shift. The contribution of this local shift to the line profile is proportional to the projected intensity at the point [24]. Intrinsic broadening effects can be accounted for by convolving the local line profile with an intrinsic Gaussian profile, yielding the result:

$$p(\lambda) = \sum_{ij} \frac{I(\theta_i, \phi_j)}{\sqrt{2\pi}\sigma} e^{-(\lambda_{ij}-\lambda)^2/2\sigma^2} \tag{4}$$

where $p(\lambda)$ indicates the corrected line profile, $\lambda$ the uncorrected wavelength, $\lambda_{ij}$ the Doppler corrected wavelength for a point on the surface given by the spherical coordinates $(\theta_i, \phi_j)$, $I$ the local intensity at this point and $\sigma^2$ the variance of the Gaussian [24]. Radial pulsations will have the effect of shifting spectral lines either to the left or right on the spectral wavelength scale, which can be corrected for. Non-radial pulsations have a more complex effect on the spectrum. The qualitative effects of pulsational modes on a line profile are dependent on the type of mode in question. Prograde sectoral modes, travelling in the same direction as the rotation, can cause the development of deep absorption features in the smooth continuum and also the narrowing of spectral lines [24]. Retrograde sectoral modes, travelling opposite to the direction of rotation, act against their prograde counterparts and diminish and disperse their effects [24]. Prograde tesseral modes (either $l - 1 = |m|$ or $l - 1 \neq |m|$) have smaller amplitudes and so have little effect other than causing 'bumps' in the line profiles of rapidly rotating stars. The strength of the bumps is inversely proportional to the degree of $l$ and the value of $l - |m|$, and so is of significance in $\gamma$-Dor stars which possess both low $l$ and high $v\sin i$ [24].

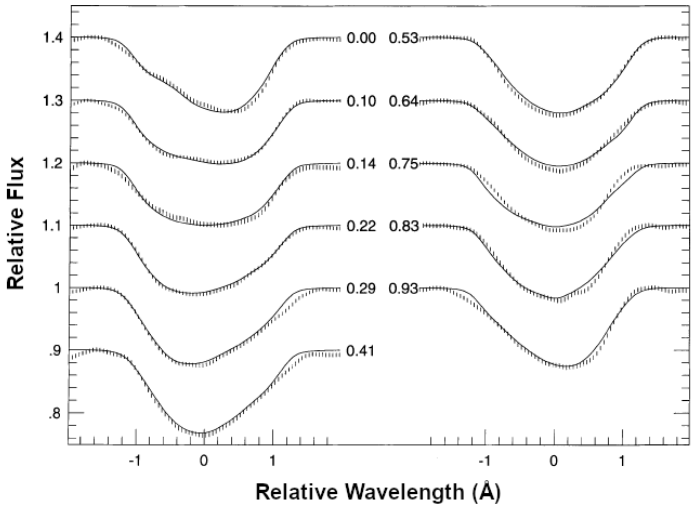


Figure 1: Illustration of line profile variations induced by pulsation in the 5318 ÅFe II line in the $\gamma$-Dor star HD 164615 [28]. The numbering on each profile indicates its pulsational phase. The solid lines represent the observed profiles while the dashed lines represent the fit to an $m = 2$ non-radial mode.

In the specific case of $\gamma$-Dor stars, the line profile is affected by low-degree, sectoral non-radial pulsation modes [28]. This induces a sequence of changes to the spectral line shapes; a blue asymmetric phase, a 'V'-shaped symmetric phase, a red asymmetric phase and a final flat-bottomed phase [28]. Overall this appears to manifest as a bump travelling along the line profile in the blue - red direction over the course of a pulsation period; an illustration of this is shown in figure 1. The characteristically high $v\sin i$ values of $\gamma$-Dor stars can complicate analysis of LPVs through velocity-induced broadening and blending of spectral lines, which is the dominant non-pulsational LPV mechanism in these stars [29]. For this reason, synthesis-based methods is often preferred for analysis of $\gamma$-Dor variables due to their increased tolerance for blending effects.

## 2.3 Synthetic Spectral Fitting Technique

The Synthetic Spectral Fitting Technique (SSFT) is a useful tool for obtaining various information from the parameter space of a spectrum. In SSFT, an attempt is made to minimise the difference between the target spectrum and a synthetic analogue, which may be either pre-prepared or generated on the fly. This is fundamentally a trial-and-error approach, with parameter values being iterated according to arbitrary adjustments until convergence is achieved [3]. Comparisons may be made across an entire spectrum or only within specified regions. iSpec is capable of generating its own synthetic spectra using a selection of synthesis codes including SPECTRUM [30] and SYNTHE [31] [1]. This approach can be more time consuming than the use of a pre-prepared spectrum, but it is also more flexible and much of the more time-intensive processes can be executed before the analysis [1]. A notable advantage of SSFT versus other methods such as Equivalent Width is that it is significantly less vulnerable to the effects of line blending, and can reproduce blends even at low resolutions [1]. This is advantageous in the study of $\gamma$-Dor stars in particular, where high radial velocities can cause significant blending [3].

iSpec allows for the determination of the stellar parameters of effective temperature, surface gravity, metallicity, micro- and macroturbulence velocities, projected equatorial

velocity, limb-darkening coefficient and spectral resolution via SSFT [1]. Effective temperature, $T_{eff}$, of a body is defined as the temperature of an equivalent black body emitting the same net amount of radiation [32]. Surface gravity is defined as the gravitational acceleration experienced on the surface of a body, it is expressed in decimal exponents (dex) obtained by expressing the acceleration in $\mathrm{cms}^{-1}$ and then taking the base-10 logarithm of this value [33]. Metallicity, as expressed by [Fe/H], is defined as the base-10 logarithm of the ratio of a star's iron abundance to it's hydrogen abundance, the corresponding solar value is then subtracted from this to give the final result [34]. Micro- and macroturbulence velocities are detailed in section 2.1 and are measured in $\mathrm{kms}^{-1}$. Projected equatorial velocity, $v\sin i$ is an expression of the rotational velocity at a point on the stellar surface in $\mathrm{kms}^{-1}$, where $v$ represents the velocity at the equator and $\sin i$ is the sine of the angle of inclination of the point [35]. Limb-darkening coefficients are coefficients used in equations to model the effects of limb-darkening, in a linear model the coefficient will determine the shape of the limb-darkening profile [36].

Once the requisite parameters have been determined, individual chemical abundances can also be found using the same method. The step sizes used for convergence in the least-squares algorithm are 100 K for $\mathrm{T}_{eff}$, 0.1 dex for log g, 0.05 dex for metallicity, 0.5 and 2.0 $\mathrm{kms}^{-1}$ for micro and macroturbulence respectively, 2.0 $\mathrm{kms}^{-1}$ for $v\sin i$, 0.2 for limb-darkening coefficient and 100 for resolution [1]. Error estimation is calculated from the co-variance matrix constructed by the least-squares algorithm. This is appropriate for atmospheric parameter errors but for abundances a more rigorous error method is preferred (as outlined in section 2.5).

## 2.4 Model Atmospheres and Line Lists

Model atmosphere grids allow various stellar parameters to be determined as a function of effective temperature and surface gravity for a given star. iSpec makes use of ATLAS [37] and MARCS [38] pre-computed model atmosphere grids as standard. The MARCS grids are formed from a combination of spherical and plane-parallel models, with the former applying to analysis of targets with a log $g$ value less than or equal to 3.5 dex and the latter applying for $3.5 < \log g \leq 5.0$. ATLAS grids are plane-parallel in all cases. For the stars considered in this study, which are of $4 \leq \log g \leq 5$, both ATLAS and MARCS should operate in plane-parallel mode and so produce similar results. MARCS covers a temperature range of 2500-8000 K while ATLAS covers 4500-8750 K. Both model atmospheres cover a metallicity range of -5.00 to 1.00 dex [1].

The pre-computed model atmospheres provide adequate coverage for the analysis of FGK stars, but by default the steps of effective temperature, surface gravity and metallicity ($\sim$ 250 K, 0.5 dex and 0.5 dex, respectively) are too coarse for detailed exploration of the parameter space [1]. The grid is refined by first linearly interpolating each value of each model atmosphere's layer from the pre-computed values, the best cases are obtained with $T_{eff}$ and log $g$ fixed both above and below the target parameters, which are then averaged [1]. A linear extrapolation is then performed, again obtaining and combining best cases with a weighted average based on the distance to the target atmosphere [1]. After the completed grid is constructed, it is simple to interpolate any atmosphere that lies between a given parameter combination. During analysis, iSpec provides only the completed grid, with any in-between interpolation being performed on-the-fly as required by the user [1].

Line lists are catalogues of reference wavelength values for various atomic transitions, used as a point of comparison in many spectroscopic procedures to identify lines in a spectrum. iSpec includes *GAIA* ESO Survey (GES) [39], Vienna Atomic Line Database (VALD) [40] and SPECTRUM line lists as standard [1]. These cover the optical range between 475-685 nm and provide a selection of medium- and high-quality lines, the exact quality of which depends on the oscillator strength and blend level [1].

## 2.5 Determination of Abundances and Uncertainties

Estimates of abundance for chemical species can be inferred from the degree of absorption from the appropriate spectral lines corresponding to ions of said species [3]. This can be done directly by integrating the flux removed from the spectrum by the lines. Assuming the relation between temperature and line strength has previously been established, deviations from this relation can then be related to the abundance. Once this has been performed for a calibration star (commonly the Sun), the line absorption of other stellar spectra can be used to determine the abundances present in different targets [3].

There are several factors that contribute to the derivation of chemical abundances via SSFT that must be accounted for when considering the uncertainties. For species with multiple spectral lines, there will be some variance in abundance values obtained from each separate line due to resolution and noise constraints. The standard deviation of these line abundances constitutes a source of uncertainty referred to as 'internal scattering', and also accounts for further uncertainties in both equivalent width and continuum normalisation [41][42]. Observational uncertainties which are also captured by the errors in the spectrum flux values themselves as well as the signal to noise ratio. For species with only one spectral line, an equivalent numerical uncertainty of 0.1 dex may be assumed [41]. Additionally, errors in the atmospheric parameters will contribute to the overall uncertainty. Ryabchikova et al (2009), following Fossati, Ryabchikova and Shulyak (2009), recommend accounting for this by considering the standard error in abundance when calculated with the parameters as given as well as with each parameter increased by $+1\sigma$ [41][42]. In the case of SSFT, $\sigma$ representing either the minimum step in the least-squares algorithm or the derived uncertainty in the parameter, whichever is larger. The parameters most significant to the result are effective temperature, surface gravity and microturbulence; total uncertainty for a given abundance $\sigma_{abn}(tot.)$ is then given by:

$$\sigma^2_{abn}(tot.) = \sigma^2_{abn}(scatt.) + \sigma^2_{abn}(T_{eff}) + \sigma^2_{abn}(logg) + \sigma^2_{abn}(v_{mic}) \tag{5}$$

Note that in equation 5, $\sigma$ does not represent the error in a given parameter, but rather the difference between the derived abundance with all parameters at their calculated value, and the derived abundance with each parameter increased by its own error.

iSpec's model atmospheres are not symmetrical in the sense that the abundance result using a given parameter $+1\sigma$ may not be the same as that when using a parameter $-1\sigma$. This error method must therefore be adapted to first determine which of $\pm1\sigma$ gives the largest uncertainty, and then incorporate that into equation 5. Using the largest uncertainty in this way could be considered as inflating the error, but in practice the difference is small and it is less computationally intensive than using both values for an asymmetric error bar. Additionally, iSpec's SSFT method generally does not produce parameter errors larger than the minimum step used in the least-squares algorithm, therefore the values of $\pm1\sigma$ to be used are $\pm100$ K, $\pm0.1$ dex and $\pm0.5$ kms$^{-1}$ for $T_{eff}$, log $g$ and $v_{mic}$, respectively.

# 3 Methodology

## 3.1 Data Collection

Stellar spectral data for this project was collected from the High Efficiency and Resolution Canterbury University Large Echelle Spectrograph (HERCULES) on the 1-m McLellan telescope at the University of Canterbury Mt. John Observatory (UCMJO), New Zealand (170°27.9' E, 43°59.2' S, elevation 1029 m [11]). HERCULES is a fibre-fed Echelle spectrograph with a wavelength range of 3800 - 8000 Å, a maximum resolving power of 70 000 and a 4096 x 4096 pixel CCD that detects the entire range in one exposure, for purposes of this study a resolving power mode of 42 000 was used. [6][11].

Data for spectroscopic standard targets were taken over the period of one month, yielding between 2 and 15 individual spectrum files per target. For the $\gamma$-Dor target, data were taken over a much longer period of several years and 327 spectra were collected in total. Data reduction was performed using the data reduction pipeline for MEGARA, a semi-automated MATLAB method maintained by Pascual and collaborators [43][44]. This code produces normalised, wavelength-calibrated and order-merged spectra, while also applying corrective procedures such as barycentric correction and cosmic ray removal [44]. In a slight modification to MEGARA, continuum normalisation was done automatically using pre-prepared, generalised templates for improved procedural efficiency.

## 3.2 Target Selection

Two types of target were required for this study. For the purposes of developing the codebase and validating the methodology, spectroscopic standard stars were used for the ease of comparison between obtained and published results. For the application of the code in a research context, the known $\gamma$-Dor star HD 135825 was chosen as its parameters have previously been studied by Bruntt et al. (2008) and Kahraman Aliçavuş et al. (2015) [6][45]. Additionally, identification of the significant pulsation frequencies in this star by Brunsden et al. (2012) allow for easy binning of spectra according to pulsation phase [11]. Details of the targets used are given in table 1.

| Target ID | Type | Spectral Class | Observation Dates | No. Spectra |
|---|---|---|---|---|
| HD 22879 | standard | G0 V [46] | Dec 2017 | 2 |
| HD 49933 | standard | F2 V [42] | Dec 2017 | 6 |
| HD 61421 | standard | F5 IV-V [47] | Dec 2017 | 15 |
| HD 135825 | $\gamma$-Dor | F0 [11] | Feb 2009 - Jun 2011 | 327 |

Table 1: Catalogue of spectroscopic standard and $\gamma$-Dor targets.

The extended observation period for HD 135825 provides a much larger dataset for analysis. This allows for fulfilment of the higher resolution requirements for the study of $\gamma$-Dor stars. This dataset is built upon that used by Brunsden et al. (2012) and was acquired using the same instrumentation and methods [11].

## 3.3 Spectral Preparation

The MEGARA pipeline produces a file containing the reduced spectral data from all observations as a function of wavelength. A python script was used to collate these

separate observations into a single, averaged spectrum for further analysis. The standard deviation of the intensity was also taken to act as a rudimentary error value. Additionally, the units of the wavelength axis were converted to nanometres from Angstroms to enable later use with iSpec. The final data is written to a .txt file in three tab-spaced columns to ensure compatibility with iSpec input file requirements.

Additional spectral processing was required before atmospheric parameters and abundances can be determined, which was carried out within iSpec itself. First, the barycentric velocity was determined from the telluric lines and then used to clean the telluric regions. No separate barycentric correction was needed as this was already performed by the reduction pipeline. Systemic radial velocity was then determined by cross-correlation to pre-existing templates and used to apply a correction to the spectrum. Signal-to-noise ratios were determined both from the reported error in the spectrum and directly from the fluxes. A continuum normalisation was then applied to the spectra of the standard stars using a median and maximum wave range of 3.0 and 4.0 nm respectively, these same values could be applied uniformly as all spectra utilised in this study were acquired from the same instrumentation. No continuum fit was applied to the spectra from HD 135825 as the normalisation applied by MEGARA was deemed sufficient in these cases. Finally, the spectra were re-sampled using linear interpolation over a total wavelength range of 424.76 to 763.21 nm.

## 3.4 Spectral Analysis

Atmospheric parameters were determined by first automatically identifying Fe I and Fe II lines using iSpec. Segments of 0.25 nm were created around each line and then parameters were determined using SSFT across all segments. The use of segments excludes non-useful areas of the spectrum and decreases computation time significantly versus analysing the entire spectral range. SSFT was performed with $T_{eff}$, log $g$, $[Fe/H]$, $v_{mic}$, $v_{mac}$ and $v\sin i$ as free parameters. Limb-darkening coefficient was fixed at 0.6, the iSpec default value and resolution was fixed at 47 000 (matching the UVES setup used in the Gaia-ESO survey and therefore the most appropriate value for the line list). Radial velocity had already been corrected and was fixed at 0. SPECTRUM code was used along with MARCS.GES model atmospheres, Solar abundances from Grevesse (2007) and a GESv5 atomic line list for all analysis runs, as these models are well-suited to analysis within the temperature and gravity range appropriate for $\gamma$-Dors. Analyses were run for a total of 6 iteration cycles [1].

Once stellar parameters were obtained, abundance determination was possible. For a given species, this was performed by finding linemasks and creating segments in the same way as previously described. SSFT analysis was then performed with all parameters fixed to their previously-derived values and the individual species abundance left as a free parameter. The returned abundances were recorded and their associated errors were retained for later use. Following Kahraman Aliçavuş et al. (2015), a list of species relevant to $\gamma$-Dor stars were chosen for analysis, ranging between Carbon and Gadolinium (Z = 6 to 64) [6].

The error in abundance was calculated using the method outlined in section 2.5. The reported error from the SSFT analysis was used as the scattering error, and then abundance determination was repeated a total of six times. This accounted for the parameters of $T_{eff}$, log $g$ and $v_{mic}$ being both increased and decreased by the minimum step used in the least-squares algorithm. The differences in abundance between each repeat and the

original run were taken and the largest difference for each parameter was taken to be that parameter's error. The parameter errors and the scattering error were then used to derive the total uncertainty in abundance according to equation 5.

## 3.5 ASPiS Automation

Performing the steps outlined in sections 3.3 and 3.4 manually in the iSpec GUI was time-consuming, however iSpec supports automation via the use of Python scripting. Automated Spectrum Processing with iSpec (ASPiS) is a suite of automation scripts created to streamline the spectrum preparation and analysis processes and simplify the user-end experience. ASPiS contains a selection of iSpec functions that are used as a Python library, this library is based on a modified version of the example.py list of functions provided with iSpec. ASPiS was built in Ubuntu 18.04 and should be compatible with any contemporaneous Debian-based unix operating system, it can be executed either in a python interpreter or in terminal. The suite consists of the function library ispec_functions.py, and three separate scripts.

The script spectrum_averager.py does not make use of iSpec, but instead produces usable averaged spectra from the MEGARA reduction pipeline output according to the process outlined in section 3.3. This is done by looping over the wavelength range of the spectra and taking the median of all recorded intensity values for a given wavelength step. The error is taken to be the standard deviation of the intensity values at each step. If desired, Julian date information encoded within the MEGARA output can be used to 'bin' the observed spectra according to the phase of pulsation during which they were taken. To do this, the user must first define the period, in days, of the relevant pulsation as well as the number of spectral 'bins' to be created. A minimum of 5 bins is recommended, fewer than this can lead to aliasing while significantly more bins will increase computation time. Binning is performed by taking the difference in Julian time between a given observation and the chronologically first (zero-point) observation. The modulo of this time interval and the pulsation period is then taken and used to assign the spectrum to a bin. For a time interval of $t$ in a pulsation period $P$ with $N$ bins, the spectrum will be assigned into bin $B$ such that:

$$\frac{(B-1)P}{N} < tmodP \leq \frac{BP}{N} \tag{6}$$

The median flux values and standard errors are then calculated for each bin as normal and the results for each bin saved as a separate datafile.

The preparatory steps are carried out by spectrum_prep.py. This requires an iSpec-compatible spectrum datafile, produced previously by the averager script, which is then converted to a .fits file. The processes of telluric cleaning, velocity correction, resolution degradation, continuum normalisation and resampling are performed using the parameters given in section 3.3 by default. Spectrum signal-to-noise ratios are determined and saved to a separate results file.

Atmospheric parameter and chemical abundance determination are performed by the final script spectrum_analyser.py. Parameters are determined exactly according to the method in section 3.4 using Fe I and Fe II lines. To allow for more valid parameter results, the 'initial guess' values for the parameters were defined in a config file, for example allowing Solar values to be used as a starting point for Sun-like stars. The parameter results are appended to the same file as the SNR results from the preparation stage along

with their errors. Abundance determination is carried out for a user-defined list of species, additionally a threshold line number may be specified, with species with fewer detected lines than the threshold being ignored during analysis to decrease computation time. The detected linemask data can be saved if desired by the user, or can be purged after analysis of the corresponding species. The error determination process has been greatly sped up by the implementation of multiprocessing, by default this executes as many processes simultaneously as there are detected cores on the machine running the code, but this can be restricted by the user if desired. As a benchmark of the effect of multiprocessing, computation time for 59 lines of Ca I in the spectrum of HD 61421 decreased from 587 seconds in series to 308 seconds when multiprocessed, for a total reduction of 48%. Final abundance values with errors are appended to the results file along with the number of detected lines for each species.

# 4 Results

## 4.1 Spectroscopic Standards

### 4.1.1 Spectrum Processing

The prepared spectra for the standard stars created via the MEGARA/iSpec/ASPiS pipeline are shown in figure 2. The spectral data ranges from 424.76 to 763.39 nm in steps of 0.002 nm, and the spectral resolution is fixed to 47 000. Due to resampling, these values are uniform across all three targets. Spectral signal-to-noise ratios were determined in two ways; from dividing the flux by the reported error in the spectrum ($SNR_{errors}$) and by homogeneously resampling the spectrum in 10x10 steps, determining the SNR for each step, then taking the mean ($SNR_{fluxes}$). The results of this are shown in table 2:

| Target | $\text{SNR}_{fluxes}$ | $\text{SNR}_{errors}$ |
|---|---|---|
| HD 22879 | 164.10 | 289.00 |
| HD 49933 | 180.63 | 222.39 |
| HD 61421 | 287.74 | 719.32 |

Table 2: Signal-to-noise ratios from errors and flux values for spectroscopic standard targets.

Note that the errors in the spectral data are taken to be the standard deviation of the individual spectrum datapoints that where averaged to create the final spectrum file for each target. This is demonstrated by the fact that HD 61421 has a significantly higher SNR from its errors, since it had the most observed spectra (see table 1) and thus its standard deviations will be the smallest.

It can be seen on the spectra in figure 2 that spectral lines are more sparse in the approximate range 680 to 750 nm. Some spectral data has been removed in this region during the process of cleaning the telluric lines. Significant drops and rises in flux are found at the red and blue ends of the spectrum respectively, likely artefacting caused at the fringes of the detection band of the instrumentation. The continuum is normalised to a fixed value of 1.0, though it can be seen that large parts of the continuum are slightly above this value and also some sections (notably in the telluric region) lie below it. This is likely the result of attempting to apply a single set of continuum fitting coefficients to

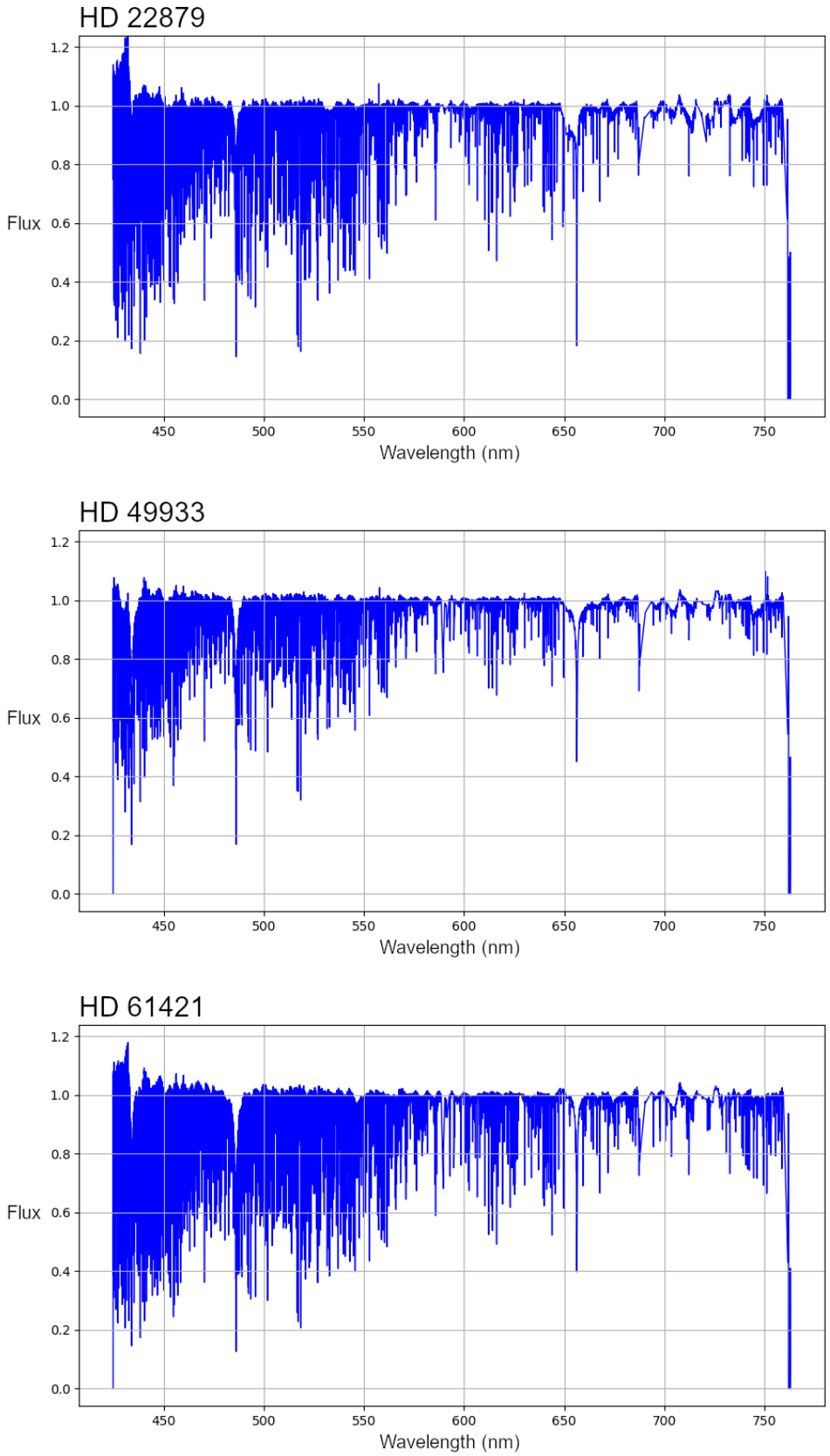


Figure 2: Processed spectra of spectroscopic standard target stars. From top to bottom: HD 22879, HD 49933 and HD 61421.

the whole spectral range, instead of taking a range of smaller continuum regions around significant lines.

### 4.1.2 Atmospheric Parameters

The validity of the methodology was tested using spectroscopic standard stars, which have are well-studied and provide many literature values as points of comparison. For atmospheric parameters, literature values of $T_{eff}$, log $g$, $v\sin i$ and $[Fe/H]$ were taken from the University of Strasbourg's SIMBAD data archive. To facilitate useful comparison, literature values were only taken from archive results that were published in or after the year 2000, obtained via spectroscopic methods and contained freely available data for all necessary parameters ($T_{eff}$, log $g$, $[Fe/H]$ and $v_{mic}$, $v\sin i$ was considered separately). The full archive dataset used is available in appendix 1. Results are shown in table 3. It can be seen that in general, the parameter values obtained from iSpec/ASPiS lie close to, or within error of the deviation range of the archive values. Notably, effective temperature results are consistently higher than literature values, which may be a systematic effect of imperfect continuum normalisation of the spectra. Surface gravity values are in good agreement with literature for all targets, as are metallicity values with the notable exception of HD 61421 which displays decreased metallicity compared to literature. Microturbulence velocities are consistent with literature values, most likely as this parameter is affected by log $g$ [6], which itself shows little discrepancy. Projected equatorial velocity values are either close to or within agreement with literature, partially because the literature values themselves have relatively large deviation since $v\sin i$ can display significant variation between separate studies. For examples of this, see the full table in appendix 1.

| Target | Parameter | This Work | Error | Literature | Literature Error |
|---|---|---|---|---|---|
| HD 22879 | $T_{eff}$ | 6071 | 100 | 5874 | 63 |
| | log $g$ (dex) | 4.4 | 0.1 | 4.4 | 0.1 |
| | $v\sin i$ ($\mathrm{kms}^{-1}$) | 3.2 | 0.9 | 1.1 | 0.9 |
| | $[Fe/H]$ | -0.81 | 0.01 | -0.83 | 0.03 |
| | $v_{mic}$ ($\mathrm{kms}^{-1}$) | 1.3 | 0.5 | 1.47 | 1.02 |
| HD 49933 | $T_{eff}$ | 6766 | 100 | 6597 | 84 |
| | log $g$ | 4.2 | 0.1 | 4.2 | 0.1 |
| | $v\sin i$ | 8.04 | 0.79 | 10.29 | 2.76 |
| | $[Fe/H]$ | -0.47 | 0.01 | -0.41 | 0.05 |
| | $v_{mic}$ | 1.7 | 0.5 | 1.96 | 0.30 |
| HD 61421 | $T_{eff}$ | 6662 | 100 | 6634 | 117 |
| *(Procyon)* | log $g$ | 4.0 | 0.1 | 4.1 | 0.2 |
| | $v\sin i$ | 3.8 | 0.5 | 4.0 | 1.0 |
| | $[Fe/H]$ | -0.17 | 0.005 | -0.013 | 0.026 |
| | $v_{mic}$ ($\mathrm{kms}^{-1}$) | 2.0 | 0.5 | 1.9 | 0.3 |

Table 3: Comparison of atmospheric parameters and errors derived in iSpec versus literature values from the SIMBAD archive and their standard deviation.

### 4.1.3 Chemical Abundances

For chemical abundances, comparisons were made to various published values for each target. For HD 61421, this included seven previous studies for a range of light elements

from carbon to iron [47]. These works are referred to here as KW96 (Kato & Watanabe 1996 [47]), TL78 (Tompkin & Lambert 1978 [48]), KS82 (Kato & Sadakane 1982 [49]), S85 (Steffen 1985 [50]), LL87 (Lane & Lester 1987 [51]), E93 (Edvardsson et al. 1993 [52]) and LH05 (Luck & Heiter 2005 [53]). These studies collectively cover a range of atmospheric parameters of 6400-6750 K for $T_{eff}$, 3.95 to 4.04 dex for log $g$ and 1.8 to 2.4 kms$^{-1}$ for $v_{mic}$. Results are shown in table 4.

| Species | N | [X/H] | Error | KW96 | TL78 | KS82 | S85 | LL87 | E93 | LH05 |
|---|---|---|---|---|---|---|---|---|---|---|
| C I | 5 | -0.02 | 0.07 | 0.22 | 0.07 | - | -0.03 | - | - | -0.05 |
| N I | 1 | 0.40 | 0.10 | 0.13 | 0.07 | - | 0.07 | - | - | - |
| O I | 1 | 0.10 | 0.10 | 0.36 | 0.07 | - | -0.08 | - | -0.05 | -0.26 |
| Mg I | 9 | -0.05 | 0.09 | -0.04 | - | -0.04 | 0.07 | -0.24 | 0.07 | 0.07 |
| Al I | 1 | 1.20 | 0.10 | -0.01 | - | -0.05 | -0.01 | 0.40 | 0.00 | -0.13 |
| Si I | 26 | -0.01 | 0.04 | -0.10 | - | 0.00 | 0.12 | -0.07 | 0.01 | 0.00 |
| Fe I | 563 | -0.16 | 0.12 | 0.00 | -0.14 | -0.01 | -0.02 | -0.11 | -0.02 | -0.04 |

Table 4: Comparison of derived chemical abundances between ASPiS-derived and literature values for HD 61421. $N$ indicates the number of spectral lines detected for a given species.

The results show both discrepancy and agreement with the literature as the abundance values between different studies can also vary significantly. The most deviant results are found for cases of low $N$, particularly with nitrogen, oxygen and aluminium; this is to be expected as SSFT becomes more accurate with increasing numbers of spectral lines, and so for the investigation of $\gamma$-Dor targets, any species with fewer than 2 spectral lines were not used. Kato & Watanabe note that their own investigation shows and apparent overabundance of CNO relative to other studies which place the abundances at around solar level. This is explained by these species not being properly in local thermal equilibrium, applying a detailed atomic physics correction to these results corrects the departure from LTE and yields near-solar values [47]. Such corrections require highly species-specific treatment which would be beyond the scope of this investigation and so were not performed. Note that Kato & Watanabe observed LTE departure due to their study focusing on strong CNO lines, the other cited studies obtained abundance from weaker lines where there are no significant departures.

For HD 49933, comparisons were taken against a study by Fossati, Ryabchikova & Shulyak (2009) [42], which in turn cites Bruntt et al. (2008) [45]. These studies are referred to as FRS09 and B08 respectively. Solar abundances for the literature values were taken from either Grevesse & Sauval (1998) or Asplund, Grevesse & Sauval (2005), denoted as GS or AGS respectively [42]. Fossati used a $T_{eff}$ value of 6500 K and a log $g$ of 4.00 while Bruntt chose 6780 K and 4.24. Results are given in table 5.

Similar to table 4, the results for HD 49933 suggest reasonable agreement with literature when accounting for the considerable variance within the literature itself. iSpec abundances are close to or within error of the literature values, and agreement may be greater if including the uncertainties in the reference results, which were not included in the published study. A standout exception is Ce II, which is significantly different from its reference point and the only reported overabundance in a series of otherwise sub-solar metallicities. Of note is the fact that the uncertainties in the iSpec/ASPiS abundance values are large, particularly in cases such as Co I and Sc II. However, in the absence of reported uncertainties in the literature values no immediate comparison can be made. The

| Species | N | [X/H] | Error | RFS09$_{AGS}$ | RFS09$_{GS}$ | B08$_{GS}$ | N$_{FRS09}$ |
|---|---|---|---|---|---|---|---|
| Mg I | 6 | -0.33 | 0.10 | -0.32 | -0.37 | - | 4 |
| Si I | 6 | -0.37 | 0.17 | -0.33 | -0.37 | -0.37 | 20 |
| Ca I | 43 | -0.31 | 0.18 | -0.28 | -0.33 | -0.50 | 26 |
| Sc II | 11 | -0.39 | 0.20 | -0.25 | -0.37 | -0.45 | 12 |
| Ti I | 24 | -0.28 | 0.12 | -0.40 | -0.52 | -0.52 | 19 |
| Ti II | 51 | -0.29 | 0.17 | -0.28 | -0.40 | -0.41 | 33 |
| V I | 3 | -0.63 | 0.18 | -0.46 | -0.46 | - | 4 |
| Cr I | 51 | -0.47 | 0.13 | -0.42 | -0.45 | -0.63 | 25 |
| Cr II | 16 | -0.42 | 0.21 | -0.21 | -0.24 | -0.43 | 16 |
| Mn I | 15 | -0.56 | 0.10 | -0.68 | -0.68 | - | 14 |
| Fe I | 325 | -0.46 | 0.13 | -0.45 | -0.50 | -0.44 | 158 |
| Fe II | 44 | -0.43 | 0.15 | -0.44 | -0.49 | -0.44 | 31 |
| Co I | 5 | -0.33 | 0.38 | -0.37 | -0.37 | - | 3 |
| Ni I | 33 | -0.57 | 0.09 | -0.53 | -0.55 | -0.48 | 41 |
| Ce II | 8 | +0.43 | 0.15 | -0.27 | -0.27 | - | 5 |

Table 5: Comparison of iSpec/ASPiS-derived abundances and literature values for HD 49933. $N$ indicates the number of detected spectral lines for a given species and $N_{FRS09}$ indicates the number of lines reported in Fossati, Ryabchikova & Shulyak (2009) [41].

number of spectral lines detected by iSpec is much greater than that from the literature in some cases, notably Fe I. This may be due to improved resolution in the MEGARA data, but also may indicate the detection and inclusion of spurious lines by iSpec.

The results for HD 22879 are given in table 6, with literature reference values are taken from Jofré et al. (2015). Comparison shows that the obtained metallicities are also generally in agreement with the literature, with Co I being the only outlier. The number of detected spectral lines is generally higher than in the literature, with notable examples being Cr I, Ni I and Ca I. Resolution is unlikely to be the explanation in this case as the literature study is relatively recent and enforced a uniform resolving power of 65 000 to all its data [54]. Possible explanations may instead by the selected wavelength range or differences in continuum normalisation methods. Uncertainties in the iSpec/ASPiS values are generally larger than the literature uncertainties, but still generally comparable. The uncertainty determination method employed by Jofré et al. was similar to that outlined in section 2.5 and equation 5, but also included an error term for metallicity [54]. Of note is the fact that Jofré et al. made use of multiple analysis methods, including iSpec [54]. Furthermore, the literature study utilised atomic data from the GES v4 line list, as opposed to the v5 list used in this project. The v5 list features an extended wavelength regime and updated laboratory log $gf$ values for several lines, including notably Fe I. Jofré et al. were also more discriminate in their selection of spectral lines, choosing ten $\alpha$ and iron-peak species possessing lines of sufficient quality (i.e. their transition properties are known with good accuracy). The combination of an earlier version of the line list and a more meticulous selection of spectral lines will also have contributed significantly toward the discrepancy in results between this study and the literature.

Overall, the results of the spectroscopic standards suggest that the results produced by the iSpec/ASPiS method are valid in the sense that they are in at least as good agreement with the literature as the literature is in agreement with itself. This is to say that results can be highly variable and uncertainties relatively large, but this is consistent with the

| Species | N | [X/H] | Error | $[X/H]_{J15}$ | $Error_{J15}$ | $N_{J15}$ |
|---|---|---|---|---|---|---|
| Mg I | 8 | -0.40 | 0.10 | -0.48 | 0.06 | 8 |
| Si I | 12 | -0.54 | 0.05 | -0.59 | 0.08 | 14 |
| Ca I | 52 | -0.50 | 0.13 | -0.53 | 0.05 | 18 |
| Ti I | 73 | -0.44 | 0.13 | -0.55 | 0.10 | 50 |
| Sc II | 13 | -0.82 | 0.11 | -0.79 | 0.08 | 8 |
| V I | 13 | -0.82 | 0.17 | -0.73 | 0.05 | 8 |
| Cr I | 83 | -0.77 | 0.13 | -0.86 | 0.09 | 16 |
| Mn I | 20 | -1.08 | 0.09 | -1.16 | 0.08 | 10 |
| Co I | 9 | -0.57 | 0.10 | -0.74 | 0.03 | 4 |
| Ni I | 70 | -0.80 | 0.09 | -0.85 | 0.09 | 22 |

Table 6: Comparison of iSpec/ASPiS-derived abundances and literature values for HD 22879. Literature values are denoted with J15 and are taken from Jofré et al. (2015) [54].

nature of studies of this type. Notably deviant species should be noted as this may be indicative of systemic issues when analysing these in particular. Additionally, species with insufficient detected spectral lines should be discounted as valid results, while the effects of spurious lines should also be taken into consideration.

## 4.2 HD 135825

### 4.2.1 Spectrum Processing

Processed spectra for HD 135825 are shown in figure 3. The spectral data covers the same wavelength range as that of the standards spectra in figure 2 with the same interval and resolution. The reported signal-to-noise ratios from errors and fluxes are 1144.89 and 745.26 respectively, these are much higher than the SNR values for the standard stars (see table 2) due to the much larger observational dataset used to create this spectrum (see table 1). Notable on the spectrum is the presence of several prominent 'spikes' in flux both above and below the continuum around 550 nm. It is speculated that these are the result of merging orders on the Echelle spectrograph. Before parameter or abundance analysis could be performed, these spikes were removed by manually altering the datafile to fix the flux of these spike regions to 1.0. As these regions were relatively narrow and also not situated in an area with many spectral lines, it was not expected that this removal process would significantly impact the parameter or abundance results. Also visible on the left-hand spectrum of figure 3 are the telluric lines, which have been removed in the processed file. The effects of resampling and resolution degradation can also be seen in the apparent reduction of the intensity of some lines, notably the H-$\alpha$ line at 656 nm.

A close-up view of one of the flux spikes at approximately 550.95 nm is shown in figure 4. The steep sloping sides of the spike and the discontinuity between them suggests that it is caused by the merging of two spectrograph wavelength orders. Figure 4 also demonstrates the necessity of manually removing these features, as despite its narrow shape, an automated analysis procedure could interpret the 'downward' side of the spike as a spectral line. Additionally, the spike could interfere with continuum fitting in this region.

The continuum fit of the spectrum should in theory normalise all the spectral flux to a value of 1.0. As can be seen in figure 5, this has not been executed perfectly in all regions. Since spectral line depth is measured from the continuum line, any line regions

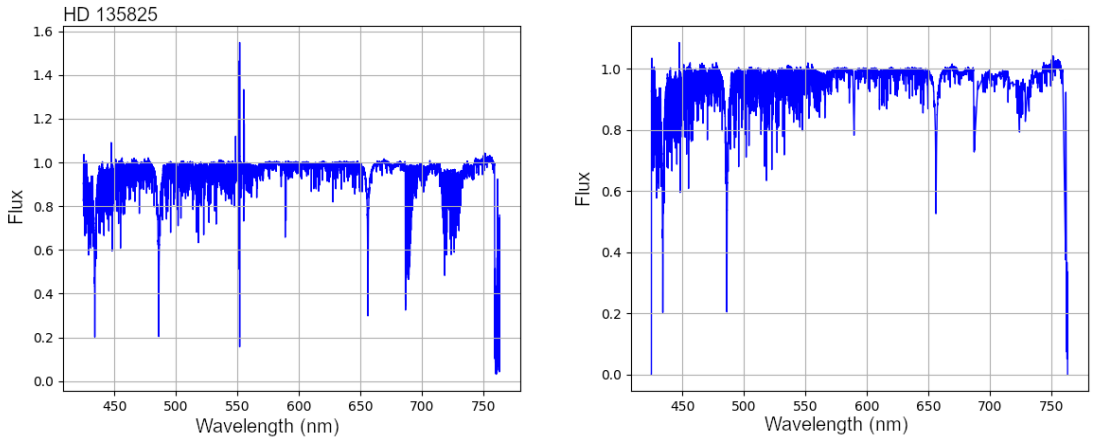


Figure 3: Spectra of HD 135825 before (left) and after (right) processing including manual removal of flux spikes.

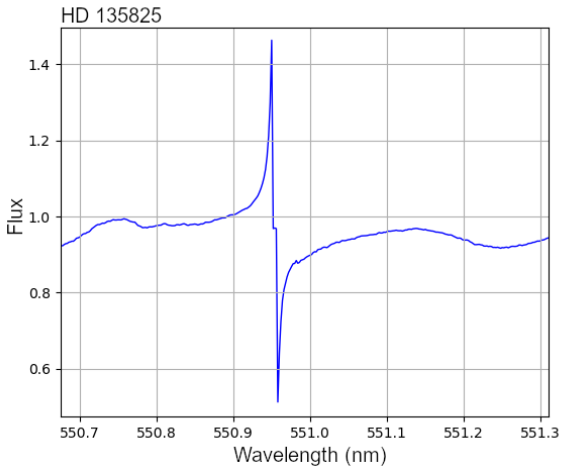


Figure 4: Detailed view of an example flux spike in the spectrum of HD 135825. The shape of the spike, as well as the small flat zone in the centre, suggests this is caused by the merging of two separate orders on the spectrograph.

lying below the continuum will have their apparent depth increased. Accordingly, any lines that lie above the line will have their depth reduced. As can be seen on figure 3, most of the spectral data for HD 135825 lies either on or slightly below the continuum level. A more suitable method for continuum normalisation may be to pre-define smaller regions of continuum across the spectrum and then perform partial fitting around these regions, rather than attempting to apply a single, uniform fit across the entire spectrum.

### 4.2.2 Atmospheric Parameters

The obtained atmospheric parameter values for HD 135825 are given in table 7. For comparison purposes, literature values taken from Bruntt et al. (2008) [45] are included as well. The effective temperature result of 7158 K is higher than, but within error of Bruntt's value and also within the typical temperature range for $\gamma$-Dors of 6500 to 7500 K [15]. The value for log $g$ is notably higher than Bruntt's value, and lies just outside of the upper limit of the typical range of 3.8 to 4.7 dex [6]. This discrepancy is possibly due

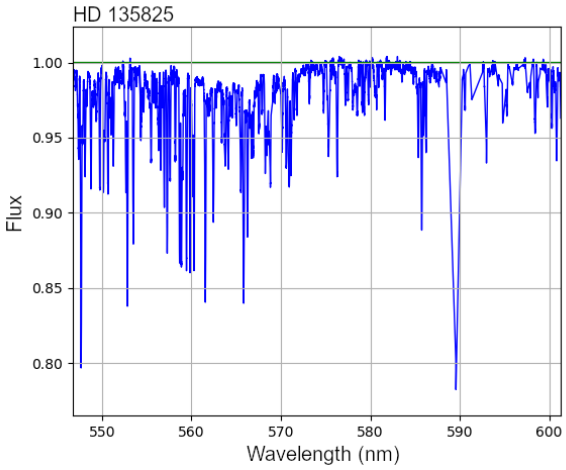


Figure 5: A demonstration of the quality of the continuum fit applied to the HD 135825 spectrum by MEGARA. The continuum is fixed at 1.0 as shown by the green line.

to differences in synthesis code and model atmosphere employed between this study and the literature, as well as imperfections in continuum fitting. Metallicity was found to be at +0.01, a slight decrease from Bruntt's value. The results are however within margin of error of each other. The projected equatorial velocity $v\sin i$ is in good agreement with literature. The microturbulence velocity is significantly higher than the literature value, this may reflect the discrepancy in log $g$, which influences microturbulence [6].

| Parameter | Value (iSpec) | Error (iSpec) | Value (Bruntt) | Error (Bruntt) |
|---|---|---|---|---|
| $T_{eff}$ (K) | 7158 | 100 | 7050 | 180 |
| log $g$ (dex) | 4.8 | 0.1 | 4.39 | 0.13 |
| $[Fe/H]$ | +0.01 | 0.05 | +0.13 | 0.09 |
| $v\sin i$ ($\mathrm{kms}^{-1}$) | 39.38 | 2.45 | 38.0 | - |
| $v_{mic}$ ($\mathrm{kms}^{-1}$) | 2.9 | 0.5 | 1.5 | 0.4 |

Table 7: Atmospheric parameters and errors derived in iSpec for the $\gamma$-Doradus star HD 135825.

### 4.2.3 Chemical Abundances

The obtained chemical abundances and errors for HD 135825 are listed in table 8. The species represented account for all species between Z = 6 and Z = 64 for which a minimum of 3 spectral lines were detected. Most results fall within a range of $-1.0 \leq [X/H] \leq +1.0$, with notable outliers including Sm II at +1.31 and Ba II at -1.38, both of which having small numbers of detected lines at 4 and 3 respectively. Fractional errors in abundance values are proportionally large in most cases, most likely due to a combination of model choice, limitations of SSFT at low $N$, and the effects of line profile variations.

### 4.2.4 Pulsational Phase Binning

The total spectral data for HD 135825, consisting of 327 individual observations, was split into 5 bins according to the pulsational phase during which each observation was taken

| Species | N | [X/H] | Error |
|---|---|---|---|
| Mg I | 4 | -0.25 | 0.11 |
| Si I | 4 | +0.51 | 0.31 |
| Ca I | 18 | +0.14 | 0.17 |
| Ti I | 20 | +0.50 | 0.23 |
| Ti II | 15 | +0.16 | 0.17 |
| V I | 8 | -0.11 | 0.46 |
| Cr I | 41 | -0.12 | 0.12 |
| Cr II | 4 | -0.41 | 0.43 |
| Mn I | 8 | 0.00 | 0.11 |
| Fe I | 82 | -0.05 | 0.10 |
| Fe II | 18 | -0.12 | 0.12 |
| Ni I | 13 | -0.18 | 0.12 |
| Ba II | 3 | -1.38 | 0.13 |
| Ce II | 7 | +0.55 | 0.47 |
| Sm II | 4 | +1.31 | 0.18 |

Table 8: iSpec/ASPiS-derived abundances and uncertainties for HD 135825

(see section 3.5. The number of spectra assigned to each bin varied between 53 and 76, as shown in table 9. If observational coverage of the pulsation period were uniform, an average of 65 spectra per bin would be expected. The reduction in dataset size caused a reduction in signal-to-noise ratio relative to that of the full dataset, with an average value calculated from the fluxes of 454. SNR from errors was not determined for the binned spectra as calculation of the spectrum errors in the binning process increased computation time prohibitively.

| | Bin 1 | Bin 2 | Bin 3 | Bin 4 | Bin 5 |
|---|---|---|---|---|---|
| No. Spectra | 76 | 53 | 63 | 65 | 70 |
| SNR | 466 | 410 | 465 | 471 | 458 |

Table 9: Distribution of observed spectral data and signal-to-noise ratio among phase bins.

### 4.2.5 Atmospheric Parameters with Binning

Atmospheric parameter values and errors for each of the 5 bins are displayed in table 10. For comparison, the values derived from the full, unbinned dataset are included. The quoted errors in the binned data are taken from the minimum step values used in the SSFT method for each parameter. Binned $T_{eff}$ values are consistently higher than the unbinned value, but with a discrepancy of 76 K at most this never exceeds the margin of error of the parameter. Conversely, log $g$ values are consistently lower than the unbinned value when binning is applied. This is most observable in bins 4 and 5, where the value drops to below 4.0. Metallicity values fluctuate about 0.00 across the bins. The binned values of $v\sin i$ are generally higher than the unbinned value with bins 4 and 5 again acting as exceptions. It is of note that the $v\sin i$ results for bins 1, 2 and 3 are in closer agreement with Bruntt's value of 38.0 than the unbinned value is. Microturbulence velocities oscillate around the unbinned value across the bins, but remain within margin of error. Macroturbulence

| Parameter | Unbinned | Bin 1 | Bin 2 | Bin 3 | Bin 4 | Bin 5 |
|---|---|---|---|---|---|---|
| $T_{eff}$ (K) | 7158 | 7167 | 7221 | 7234 | 7232 | 7188 |
| error | 100 | 100 | 100 | 100 | 100 | 100 |
| log $g$ (dex) | 4.8 | 4.5 | 4.1 | 4.2 | 3.9 | 3.6 |
| error | 0.1 | 0.1 | 0.1 | 0.1 | 0.1 | 0.1 |
| $[Fe/H]$ | +0.01 | +0.13 | -0.04 | +0.05 | -0.07 | 0.00 |
| error | 0.05 | 0.05 | 0.05 | 0.05 | 0.05 | 0.05 |
| $v\sin i$ (kms$^{-1}$) | 39.38 | 36.21 | 39.92 | 36.49 | 23.91 | 29.09 |
| error | 2.90 | 2.00 | 2.00 | 2.00 | 2.00 | 2.00 |
| $v_{mic}$ (kms$^{-1}$) | 2.88 | 2.80 | 3.19 | 2.42 | 3.35 | 2.35 |
| error | 0.50 | 0.50 | 0.50 | 0.50 | 0.50 | 0.50 |
| $v_{mac}$ (kms$^{-1}$) | 48.5 | 50.0 | 36.2 | 33.2 | 50.0 | 45.6 |
| error | 2.2 | 2.0 | 2.0 | 2.0 | 2.0 | 2.0 |

Table 10: Atmospheric parameter values and uncertainties derived for HD 135825 with the spectral data separated into 5 bins according to pulsation phase.

velocities are generally lower than the unbinned value with the exception of bins 1 and 4, however the flat value of 50.0 for these bins may indicate some kind of model-limited maximum value and therefore should not be regarded as reliable.

### 4.2.6 Chemical Abundances with Binning

| Species | Bin 1 | | Bin 2 | | Bin 3 | | Bin 4 | | Bin 5 | |
|---|---|---|---|---|---|---|---|---|---|---|
| | Value | Error | Value | Error | Value | Error | Value | Error | Value | Error |
| Mg I | +2.79 | 4.70 | - | - | - | - | - | - | -0.01 | 1.14 |
| Si I | +0.13 | 2.47 | -0.06 | 4.97 | +0.05 | 1.33 | - | - | +0.41 | 2.72 |
| Ca I | +0.22 | 1.21 | +0.20 | 1.54 | +0.21 | 1.52 | +0.14 | 1.13 | +0.28 | 1.89 |
| Ti I | +0.18 | 1.40 | +0.16 | 1.21 | +0.02 | 1.62 | +0.03 | 1.37 | +0.26 | 1.43 |
| Ti II | +0.21 | 0.84 | +0.16 | 1.01 | +0.11 | 1.08 | -0.01 | 0.85 | +0.01 | 1.30 |
| V I | - | - | +0.03 | 3.92 | +0.32 | 4.26 | +0.10 | 3.68 | - | - |
| Cr I | -0.04 | 1.04 | -0.06 | 1.04 | -0.18 | 1.25 | -0.14 | 0.87 | +0.04 | 1.23 |
| Cr II | -0.22 | 2.37 | - | - | - | - | - | - | -0.04 | 2.32 |
| Mn I | -0.03 | 2.04 | +0.16 | 3.04 | -0.04 | 3.72 | -0.13 | 3.80 | -0.07 | 2.50 |
| Fe I | +0.07 | 0.32 | -0.05 | 0.30 | +0.04 | 0.36 | -0.10 | 0.33 | -0.01 | 0.34 |
| Fe II | +0.06 | 0.72 | +0.12 | 0.79 | +0.09 | 0.94 | -0.02 | 0.71 | +0.03 | 0.74 |
| Ni I | -0.20 | 1.69 | +0.03 | 1.71 | +0.08 | 1.88 | +0.06 | 1.42 | -0.12 | 1.35 |
| Ba II | -0.89 | 4.18 | -0.64 | 3.03 | - | - | -1.02 | 2.86 | - | - |
| Ce II | - | - | +0.91 | 1.43 | +0.92 | 1.59 | - | - | +0.82 | 2.92 |
| Sm II | +0.90 | 4.34 | +1.07 | 2.43 | +1.01 | 2.49 | +0.87 | 3.26 | +0.98 | 2.13 |

Table 11: Determined chemical abundances and errors for HD 135825 with the spectral data separated into 5 bins according to pulsation phase. Values of '-' indicate no valid result was present for a species in a given bin.

Abundance results and uncertainties from the binned data are displayed in table 11. The reported error values for all results are large due to the reduced dataset for each bin compounded with the already large fractional errors in the full data as displayed in table

8. Particularly extreme outliers, as well as species with insufficient spectral lines have been omitted from the table.

# 5 Discussion

## 5.1 Analysis of Spectroscopic Standards

The analysis results for the atmospheric parameters and chemical abundances of the spectroscopic standard stars HD 22879, HD 49933 and HD 61421 show generally good agreement with established literature values. This suggests the obtained results from the iSpec/ASPiS method are valid and that the choices of model atmosphere, synthesis code, linelists etc. are well-suited to the study of such stars. The sample standard stars represent F- and G-class stars with no significant pulsations and low $v\sin i$ values. This implies that the spectra of such stars will be relatively free from line profile variation effects caused by rotation or pulsation, and thus the degree of broadening and blending is less severe than in other types of star, such as $\gamma$-Dor variables. Good results can therefore be obtained from relatively small spectral datasets, for example the processed spectrum of HD 22879 shown in figure 2 was compiled from only 2 observations. This is advantageous since practical concerns may prevent the collection of large observational datasets in some instances.

Of note is the fact that HD 61421 (Procyon A) is known to exist in a spectroscopic binary with the white dwarf star BD+05 1739B (Procyon B), with an orbital period of approximately 40.8 years [55]. While binary orbits impose a periodic shifting effect on spectral lines, due to the brevity of the observational period (1 month) in comparison to the orbital period, it is unlikely that this will have caused inconsistencies within the spectra obtained for this study. Additionally, recent data from CoRoT and TESS indicate a degree of variability in the light curve of HD 49933, believed to be indicative of surface magnetic effects [56]. This may influence the wavelengths of certain magnetically-sensitive spectral lines, such as Fe I 5250.2 Å[57], but given the large number of lines used in the analysis of each species, it is not expected that this will have a significant impact on the spectroscopic results as a whole.

### 5.1.1 Atmospheric Parameters of Standard Stars

The good agreement between the literature and obtained values for the effective temperature and surface gravity of the standard stars is significant as these parameters are most significant to the validity of the model atmosphere. Accurate values of $T_{eff}$ and $\log g$ allow for more precise interpolation of the model atmospheric grid, which in turn will improve the accuracy of any further information determined using this grid, such as other parameters or abundances. While all $T_{eff}$ results were within margin of error of their literature counterparts, the obtained values from iSpec were consistently higher. A potential reason for this is differences in modelling methods between studies. Alternatively, spectral lines may be being artificially deepened by imperfect continuum fitting, similar to that shown in figure 5 for HD 135825. Since iSpec measures line depth from the continuum level, any line lying below the continuum will have its flux artificially increased, which could then be interpreted during parameter determination as an increase in temperature.

Measurements of the projected equatorial velocity $v\sin i$ can vary highly between studies and are sensitive to systematic choices in the methodology employed. This can make

it difficult to calibrate the resultant line broadening, which is of particular concern in stars that rotate rapidly. However, when $v\sin i$ is low, the low degree of induced LPVs will mean that a low precision in the parameter will have a much smaller impact on the quality of results than more crucial parameters such as $T_{eff}$ and log $g$. The agreement of the iSpec/ASPiS values for $v\sin i$ with literature is therefore more reflective of the difficulty in obtaining consistent values for this parameter than the precision of the analysis methods used in this work. The obtained values of $v\sin i$ for these stars have evidently not had a significant impact on the determination of the results of other parameters or abundances.

The derived metallicity value of HD 61421 is of significance due to its unique discrepancy from the literature value, which itself is well-defined and has a small margin of error. A possible explanation for this is a difference in solar abundances used in analysis, but given the significant amount of reference data and the well-defined nature of solar abundances this is unlikely. The spectrum of HD 61421 in figure 2 displays a notable amount of 'overlap' above the continuum level. This could cause underestimation of the flux of iron lines in these regions. coupled with the flux in the Balmer lines, which are closer to the continuum level, could lead to an apparent decrease in [Fe/H]. It is of note however that the spectra of HD 22879 and HD 49933 also display similar continuum overlap and do not display such deviation from their literature values. However this may be because their literature metallicities are already significantly lower than that of HD 61421. There may be a link between the reduced [Fe/H] value and the relatively low $T_{eff}$ value obtained for HD 61421. Both other spectroscopic standards obtained metallicities consistent with literature but had reported temperatures $\sim$200 K greater than expected. If this trend were applied to HD 61421, the expected result would be about 6800 K, this may compound with the slightly lowered log $g$ measurement to affect the grid interpolation of the model atmosphere and hence the determined value of metallicity.

Microturbulence values are in good agreement with literature for all three standard stars. For AFG stars it is known that microturbulence velocity is correlated with surface gravity such that a higher log $g$ implies a lower $v_{mic}$ value [58]. The quality of result for microturbulence may therefore be a reflection of the similarly good agreement in log $g$ values. The correlation between the two parameters can also be seen across the 3 standards, with HD 22879 having the highest log $g$ and lowest $v_{mic}$, while HD 61421 conversely has the lowest log $g$ and highest $v_{mic}$. Accurate knowledge of turbulent velocities is important for line profile analysis in stars similar to the standards, as the absence of significant pulsationally- or rotationally-induced broadening will increase the relative importance of micro- and macroturbulent broadening effects.

Overall, the parameter results are of good quality and reliability for the spectroscopic standards. The compatibility of the results with the well-established literature values imply validity for the data collection, reduction, processing and analysis methods employed. As long as the spectral data is of sufficient quality and resolution, analysis should produce accurate results. However, particular care should be taken when performing continuum normalisation as this may have an impact on the temperature and metallicity values in particular. There is indication from the results for HD 61421 that the apparent systematic overestimation of effective temperature is in fact necessary to obtain accurate results for other parameters.

### 5.1.2 Chemical Abundances of Standard Stars

For the reliable (i.e. $N > 1$) species abundance results for HD 61421, values are generally around solar levels. This is generally consistent with previous studies, as seen in table

4, which also find approximately Sun-like abundances for these species. The comparison study by Kato & Watanabe (1996) found an overabundance of Carbon, and attributed this to non-LTE effects in the strong lines they studied [47]. The lack of such overabundance in the iSpec/ASPiS results for C I suggests either an absence of these effects (indicating the presence of weak lines), or that the SSFT method is not strongly affected by non-LTE effects (so long as the lines being analysed are not sensitive to non-LTE conditions). The single-line species N I and Al I display such discrepancy from literature values that it was concluded that species with $N = 1$ should be excluded from all future analyses. For this reason, the abundance of O I must also be discounted as reliable even though it is within agreement of some literature values. If analysis of these low-$N$ species were to be carried out, it may be more appropriate to utilise an equivalent width approach on the individual lines. SSFT benefits from the use of larger numbers of detected linemasks as this enables the construction of a more accurate synthetic spectrum. Analysis of single lines via SSFT within the iSpec framework is generally only effective for very large and prominent spectral features, such as the Balmer lines.

The abundance results for HD 49933 show good agreement with the literature for most species. However, the fractional uncertainties of these results are relatively high. This is because the error approach adopted (see section 2.5) combines many sources of uncertainty in quadrature, producing larger errors overall. This is deliberate, as an attempt to account for as much of the systematic and statistical errors from the entire data collection and analysis process in a single value. This is also reflected in the variation between literature values, both for HD 49933 and other targets, a relatively large uncertainty is therefore not unexpected. A notable outlier in the abundances is that of Ce II, which is the only reported overabundance and also not in agreement with the literature. Attributing the measurement to an incorrect hydrogen abundance is also unlikely to be valid due to the good accuracy of other abundances in the star. A high abundance of cerium is unexpected as it has relatively few stable isotopes and nucleosynthesis in stars is achieved by the s- and r-processes, neither of which would be expected to occur strongly in HD 49933 [59]. However, an overabundance relative to Solar values is perhaps not anomalous as HD 49933 is approximately 2 Gyr younger than the Sun [60]. It is possible therefore that the star was either seeded with a larger initial amount of Cerium and/or that the isotopes present in the star have had less time to decay. The result may therefore be indicative not of a high abundance in HD 49933, but of a low abundance in the Sun.

The literature values used for comparison with the abundance results for HD 22879 represent the most relevant point of contrast for the iSpec/ASPiS methodology of any of the standard star literature results. This is because the analysis methodology employed in obtaining these results is the most similar to the methods used in this study. In particular, the use of SSFT via iSpec and the employment of an almost identical error determination method to that outlined in section 2.5 are of importance. The smaller uncertainty values obtained by Jofré et al may therefore indicate steps that can be taken to improve the iSpec/ASPiS pipeline. Jofré et al utilised a GES line list, but refined it by excluding all lines that are flagged as being of low-quality [54]. Additionally, line selection in the spectra was carried out separately in the 480-680 and 848-875 nm ranges, employing a more highly discriminatory approach than the automatic line detection process in iSpec. This is reflected in the lower values of $N$ obtained by Jofré et al as shown in table 6. The usage of a smaller, but more reliable and high-quality list of line masks in abundance analysis may be a potential improvement to the ASPiS method.

Like the parameter results, the results for chemical abundances suggest that the

MEGARA/iSpec/ASPiS pipeline is capable of competent spectroscopic analysis of stars of this type. The error values of the abundances will tend to be fractionally large, but this is consistent with the often-significant variation in abundance results between different studies. Differences in selection of synthesis codes, model atmospheres and line lists as well as differences in methodology can have a significant impact on derived chemical abundances. Therefore for best results, either the exact choice of methodology should be carefully considered or multiple methods should be utilised and contrasted to determine the most suitable approach.

## 5.2 Analysis of HD 135825

The results of analysis for HD 135825 show less agreement with literature than the standard stars. This may suggest that the iSpec/ASPiS method is less applicable to $\gamma$-Dor stars, or may be due to HD 135825 not being as well-studied as the spectroscopic standards, and thus the reference values are less well-established. Unlike the standard stars, HD 135825 possesses a higher equatorial velocity as well as the characteristic $\gamma$-Dor pulsations, which will induce line profile variations that are not present in the standards. Additionally, HD 135825 is significantly hotter, though still cooler than the 8000 K upper-limit of the iSpec model atmospheres. At 327 observations, the dataset for HD 135825 was significantly larger than that used for any of the standards. If the analysis results are an indication that datasets of this size or larger are required, that will imply a significant increase in observing difficulty.

### 5.2.1 Atmospheric Parameters of HD 135825

The derived effective temperature of HD 135825 is elevated with respect to the literature value, but is still within acceptable margins for $\gamma$-Dor stars. This is consistent with the trend of iSpec/ASPiS producing modestly higher temperature values than expected. This effect may be ascribable to imperfect continuum fitting, but it could also be symptomatic of some kind of systematic bias towards higher temperatures in the models used. In general however, these temperature increases are not large enough to cause provable negative impact on the quality of other parameter or abundance results.

The discrepancy in log $g$ values between this study and literature are harder to account for. The derived value of 4.8 is both significantly higher than the literature value and also lies outside the expected range for $\gamma$-Dor stars. Unlike the $T_{eff}$ results, this cannot be explained by a systematic bias of some kind as none of the standard stars displayed similar discrepancies in surface gravity. It is also unlikely that the value from Bruntt et al. is an underestimate of the true log $g$ as it lies within the expected range for $\gamma$-Dors and is consistent with other studies of similar stars. It is likely that the elevated log $g$ result has compounded with the high $T_{eff}$ result to influence the accuracy of the derivation of other parameters and abundances, as these are the two most significant parameters for atmospheric grid interpolation. Of note is that the increase in log $g$ has not caused a subsequent decrease in the value of $v_{mic}$. Microturbulence is instead significantly elevated relative to the literature value, which will accordingly indicate a higher degree of turbulent line broadening in the spectrum. For a $\gamma$-Dor star however, it would be expected that the pulsational and rotational broadening mechanisms would be more significant and constitute the dominant forms of broadening. A possible interpretation is that the increased $v_{mic}$ value is caused by the synthesis code attempting to account for the rotational or pulsational broadening effects by attributing them to turbulence instead.

The determined value of $v\sin i$ is in line with the expected range for $\gamma$-Dor stars of this type. It should be noted that to obtain an accurate value for $v\sin i$ it was necessary to set the initial guess for the parameter in ASPiS to a similarly high value; if left at the low iSpec default value of $6\,\mathrm{kms}^{-1}$, good agreement with the literature will not be reached within 6 iterations. Therefore to achieve best results with iSpec, it is recommended to have a resonably-accurate initial guess, as the iteration steps for $v\sin i$ value are not suitable for stars with higher velocities.

The metallicity of HD 135825 was found to be lower than the literature value but still within margin-of-error. If the value is an underestimate, this would run counter to expectation. Assuming the discrepancy is caused by imperfect continuum fitting affecting the reported flux of spectral lines, since the spectrum in general falls below the continuum line (see fig 5) it would be expected that the result would in fact be an overabundance due to added flux. A possible alternative method for calculating metallicity would be to use the equivalent width method on the Balmer lines, which are less susceptible to blending effects. In the case where a line is heavily blended, EW may still be used by first fitting a gaussian profile to the spectral line to more accurately fix the line position, depth and FWHM [61].

The parameter results for HD 135825 are less convincingly accurate than those for the spectroscopic standards. This may indicate problems with the methodology when applied to $\gamma$-Dor-type stars. For instance, while iSpec is designed primarily for analysis of FGK stars [1], $\gamma$-Dors lie at the boundary between A- and F-class and so may have parameters outside the range at which iSpec operates optimally. Both MARCS and ATLAS model atmosphere grids should be valid over the parameter ranges typical of $\gamma$-Dors, but the synthesis codes may have difficulty accounting for the high rotational velocities. The main obstacle for the codes is seemingly to differentiate the LPV effects of rotation from those of turbulence and other factors.

### 5.2.2 Chemical Abundances of HD 135825

Similar to the parameter results, the validity of the derived chemical abundances for HD 135825 is questionable. The results show a mixture of over- and underabundances relative to Solar levels, which is in line with expectations since the overall metallicity was reported to be Solar by the parameter analysis. Fractional errors remain large, for the same reasons as discussed for the abundances of the spectroscopic standard stars. The numbers of spectral lines detected are generally lower than those for the same chemical species in the standard stars. For example, Fe I had 82 detected lines in HD 135825 versus 325 in HD 49933 and 563 in HD 61421. This may be the result of line profile variations preventing the proper identification of all spectral lines for a species. The comparison stars are also cooler and rotate much more slowly than HD 135825. The spectra will therefore display shallower lines but with less rotationally-induced shifting, which may make the lines easier to detect due to their closer correspondence to the reference wavelengths. Given the large errors in the abundance results, the general conclusion that can be drawn is that abundances are generally around Solar levels in HD 135825. There are some exceptions to this, notably Ba II and Sm II that represent significant under- and overabundances respectively, however both species have low $N$ and so the accuracy of these measurements is debatable.

### 5.2.3 Effects of Pulsational Phase Binning

In total, the spectral data was divided into 5 bins, each corresponding to one fifth of the pulsational period of 1.315 days. As shown in table 9, observational coverage was not exactly even across the period and bins 1 and 5 received more observation time than average while bin 2 received less. 5 is the recommended minimum amount of bins for analysis of this sort, a smaller amount would be too few bins to infer any useful conclusions while a larger amount would spread the dataset too thin. The results for both atmospheric parameters and chemical abundances show variation both between bins and between the binned and unbinned data. This consideration of the effects of pulsational phases of observation is relatively novel and so there are comparatively few points of comparison available for the conclusions drawn therefrom.

The variance in surface gravity across the bins may be indicative of influence of the pulsation phase on observation, with log $g$ apparently decreasing in magnitude across a period; a similar reduction is also visible in $v\sin i$. Given the degree of accuracy of the binned results, it is likely that the potential pulsational effects on log $g$ actually influence the fitting of the parameter during analysis rather than the actual observed parameter itself. There is no strong evidence of periodicity in the other atmospheric parameters that could be caused by the pulsations themselves. Metallicity and microturbulence do display oscillatory values but this does not correspond to the pattern that would be expected from one pulsation period. Additionally, the binned results remain within error of the 'average' value as taken from the unbinned data. No significant variation in effective temperature is seen, which is in line with expectation as the small magnitude of $\gamma$-Dor pulsations would not be expected to cause significant changes in a star's radiation output. There is little obvious correlation between parameters, even in cases such as log $g/v_{mic}$ where a relation might be expected. There is some evidence to suggest that bins with higher $T_{eff}$ values have reduced metallicity results. This supports the conclusion that ASPiS has a bias towards higher temperatures that nontheless is necessary for accurate determination of other parameters.

The reported chemical abundance results are hampered by their significantly large error values. While this could be ascribed to the reduced datasets, it is noted that good results were achieved for abundances in standard stars using as few as 2 observational spectra. This suggests that there is some quality of $\gamma$-Dor stars, possibly their high rotation speeds, that necessitates larger datasets for analysis. Despite the uncertainties, some species such as Ca 1 display relative consistency in abundance across bins. Similar to the parameters, there is no evidence of any kind of pulsational variability in abundances across a period. If pulsation does have an effect on abundances, it is likely to be indirectly through first affecting parameter values. The resulting effect this would have on derived abundances is dependent on the models employed and how they cope with line profile variations.

## 5.3 The Validity of the iSpec/ASPiS Method

The results obtained from the spectroscopic standards and the $\gamma$-Doradus variable HD 135825 support the conclusion that the iSpec/ASPiS pipeline produces good results for the spectroscopic analysis of FGK stars with low projected equatorial velocities. When considering $\gamma$-Dors, or other stars with higher temperatures and/or velocities, the validity of results becomes less certain. Atmospheric parameter determination is generally performed well, though there is a systematic tendency towards slightly elevated effective

temperatures, this does not have a significant impact on the other derived results. The analysis was performed using SPECTRUM synthesis code with a MARCS.GES model atmosphere and a GES linelist. These choices of models and data were made as they provided good coverage of the expected parameter space relevant to the study of $\gamma$-Dor stars. MARCS.GES provides a narrower range of parameters than ATLAS9 (the alternative model included with iSpec), but features smaller intervals in the grids, allowing for finer interpolation. The GES linelist was selected due to its suitable wavelength regime of 420-920 nm and inclusion of hyperfine structure and isotopes that are absent from the alternative VALD list in iSpec. SPECTRUM was selected from the synthesis code options due to its superior performance over the alternatives, with codes such as MOOG not running successfully within the iSpec installation employed. iSpec does allow for the addition of codes and models not bundled with the package by default, but this was considered to be beyond the scope of this study.

To obtain best results, care should be taken during the preparation of the spectra. In particular, care must be taken when applying the continuum fit and normalisation to avoid negatively influencing the apparent flux of the spectral lines. If possible, it may be preferred to apply a variable fit to different regions of the spectrum rather than a single uniform fitting across the entire wavelength range. At present, this cannot easily be performed within the ASPiS framework and so such a fitting would need to be applied prior to analysis. Furthermore, the linemasks detected by iSpec should be inspected within the GUI to ensure that spurious lines caused by blending or other processes are not influencing analysis. For the determination of the atmospheric parameters, it may be advantageous to attempt to obtain results via the equivalent width method using the Balmer hydrogen lines. This could be paired with SSFT of the Fe 1 and 2 lines to improve results.

## 5.4 Potential Refinements and Future Work

It is clear from the conclusions of this study that there are some areas in which the ASPiS code can be improved. From an efficiency standpoint, multiprocessing could be implemented in the binning process of the spectrum preparation to improve computation times and allow for the addition of flux errors, which are currently omitted. While the code base currently supports the SPECTRUM and SYNTHE synthesis codes, it could be expanded to include the other options compatible with iSpec such as TURBOSPECTRUM or MOOG [1]. Additionally, functionality to allow parameter determination by equivalent width method should be implemented, most likely utilising the Balmer lines or similarly important equivalents such as the Calcium K-line.

Further work on this topic should focus on the goal of improving the quality of the results for $\gamma$-Dor stars without increasing the data requirements. This could be accomplished by treating the spectra more thoroughly during the continuum fitting stage as outlined in section 6.2. Furthermore, multiple combinations of model atmosphere and synthesis code should be investigated to determine the most suitable approach. If the reliability of $\gamma$-Dor results is improved, more detailed investigation into the effects of pulsation can be carried out. For example, the number of phase bins could be increased to achieve a more detailed picture of the variation in parameters or abundances across a period. The completion of more spectroscopic studies of $\gamma$-Dor stars will also broaden the corpus of reference values, and thus allow for more rigorous validation of future studies.

# 6 Conclusions

Spectroscopic analysis has been performed to successfully obtain atmospheric parameter and chemical abundance results for the standard stars HD 22879, HD 49933 and HD 61421 as well as the $\gamma$-Dor star HD 135825. To achieve this, the ASPiS automation suite was created to facilitate streamlined, user-friendly analysis using iSpec analysis software. Strong agreement with literature values for the standard stars has verified the validity and accuracy of ASPiS and demonstrated its usefulness as an analysis tool. The analysis of HD 135825 yielded parameter and abundance results that contribute to the body of extant literature on this star and can be used to improve the accuracy of future observations.

The observational data for HD 135825 were analysed both as a whole and also separated according to their pulsational phase. The binning of spectral data according to phase to investigate the effects of pulsations on the atmospheric parameters and chemical abundances was a novel approach to analysis of $\gamma$-Dors. The scope and nature of the results mean that there is not sufficient grounds to conclusively establish any effects. However, evidence has been found to suggest that the pulsation phase at which an observation is taken may influence the fitting of certain parameters, namely $\log g$ and $v\sin i$. This could have potential ramifications for future spectral studies of $\gamma$-Dor variables which make use of large datasets spread broadly across the pulsation period. Adjustments to methodology may be needed to ensure that the pulsational variations in different segments of the dataset are accounted for and do not impact analysis of the data as a whole.

To build upon the foundation established by this study, further work into mode identification in known $\gamma$-Dors is needed to then allow the phase of observations of these stars to be considered. Additional observations will then allow for the consideration of pulsation phase in targets across the $\gamma$-Dor population which will allow the potential relations identified in this work to be investigated further, as well as the possible discovery of other pulsational effects. The application of asteroseismological concerns to conventional spectroscopic methods therefore could have profound implications on the planning, execution and results of future observational works.

# References


[1] Blanco-Cuaresma S. et al. Determining stellar atmospheric parameters and chemical abundances of FGK stars with iSpec. *Astronomy & Astrophysics*, 569:A111, September 2014.

[2] Dunham T. Methods in stellar spectroscopy. *Vistas in Astronomy*, 2:1223 – 1283, 1956.

[3] Gray D.F. *The Observation and Analysis of Stellar Photospheres*. Cambridge University Press, 3rd edition, 2005.

[4] Ho P. Astronomical spectroscopy. *Encyclopedia of Astronomy and Astrophysics*, 2000.

[5] Uytterhoeven K. et al. The Kepler characterization of the variability among A- and F-type stars. I. General overview. *Astronomy & Astrophysics*, 534:A125, October 2011.

[6] Kahraman Aliçavuş F. et al. Spectroscopic survey of $\gamma$ Doradus stars - I. Comprehensive atmospheric parameters and abundance analysis of $\gamma$ Doradus stars. *Monthly Notices of the Royal Astronomical Society*, 458:2307–2322, May 2016.

[7] Cousins A.W.J and Warren P.R. Variable stars observed during the cape bright star programme. *Monthly Notes of the Astronomical Society of South Africa*, 22:65, 1963.

[8] Kaye A.B. et al. Gamma doradus stars: Defining a new class of pulsating variables. *Publications of the Astronomical Society of the Pacific*, 111:840–844, July 1999.

[9] Grigahcène A. et al. Hybrid $\gamma$ Doradus-$\delta$ Scuti pulsators: New insights into the physics of the oscillations from Kepler observations. *The Astrophysical Journal*, 713:L192–L197, April 2010.

[10] Guzik J.A. et al. Driving the gravity-mode pulsations in $\gamma$ Doradus variables. *The Astrophysical Journal*, 542:L57–L60, October 2000.

[11] Brunsden E. et al. Spectroscopic pulsational frequency identification and mode determination of $\gamma$ Doradus star HD 135825. *Monthly Notices of the Royal Astronomical Society*, 422:3535–3545, June 2012.

[12] Cox A.N. et al. Pulsations of white dwarf stars with thick hydrogen or helium surface layers. *The Astrophysical Journal*, 317:303–324, June 1987.

[13] Cox A.N. in. *New Perspectives on Stellar Pulsation and Pulsating Variable Stars*, volume 139. 1993.

[14] Blanco-Cuaresma S. Modern stellar spectroscopy caveats. *Monthly Notices of the Royal Astronomical Society*, 486:2075–2101, June 2019.

[15] Bradley P.A. et al. Results of a search for $\gamma$ Dor and $\delta$ Sct stars with the Kepler spacecraft. *The Astronomical Journal*, 149(2):68, January 2015.

[16] Qian S.-B. et al. Physical properties of $\gamma$ Doradus pulsating stars and their relationship with long-period $\delta$ Scuti variables. *Research in Astronomy and Astrophysics*, 19(1):001, January 2019.

[17] Van Reeth T. et al. Gravity-mode period spacings as a seismic diagnostic for a sample of $\gamma$ Doradus stars from Kepler space photometry and high-resolution ground-based spectroscopy. *The Astrophysical Journal Supplement Series*, 218(2):27, June 2015.

[18] Aerts C., Mathis S. and Rogers T.M. Angular momentum transport in stellar interiors. *Annual Review of Astronomy and Astrophysics*, 57(1):35–78, 2019.

[19] Lovekin C.C. and Guzik J.A. Convection and overshoot in models of $\gamma$ Doradus and $\delta$ Scuti stars. *The Astrophysical Journal*, 849(1):38, October 2017.

[20] Ouazzani R.M. et al. $\gamma$ Doradus stars as test of angular momentum transport models. *Astronomy & Astrophysics*, January 2018.

[21] Mihalas D. *Stellar Atmospheres.* 2nd edition, 1978.

[22] Gainutdinov R.Kh. and Al'Miev I.R. Natural broadening of atomic spectral lines and generalized operator of electromagnetic interaction. *Publications of the Astronomical Observatory of Belgrade*, 57:43–46, September 1997.

[23] Huang S.-S. On the Doppler broadening of absorption lines by turbulence and by multiple interstellar clouds. *The Astrophysical Journal*, 112:399, November 1950.

[24] Aerts C. and Waelkens C. Line profile variations of rotating pulsating stars. *Astronomy & Astrophysics*, 273:135, June 1993.

[25] Kochukhov O. Pulsational line profile variation of the roAp star HR 3831. *Astronomy & Astrophysics*, 446:1051–1070, 2006.

[26] Hao J. Line profile analysis of nonradial pulsation modes based on Doppler imaging. *The Astrophysical Journal*, 500:440–448, June 1998.

[27] Gizon L. and Solanki S.K. Determining the inclination of the rotation axis of a Sun-like star. *The Astrophysical Journal*, 589:1009–1019, June 2003.

[28] Hatzes A.P. Spectral line profile variations in the gamma Doradus variable HD 164615: non-radial pulsations versus star-spots. *Monthly Notices of the Royal Astronomical Society*, 299:403–409, September 1998.

[29] Balona L.A. et al. Line profile variations in $\gamma$ Doradus. *Monthly Notices of the Royal Astronomical Society*, 281(4):1315–1325, August 1996.

[30] Gray R.O. and Corbally C.J. The calibration of MK spectral classes using spectral synthesis. 1: The effective temperature calibration of dwarf stars. *The Astronomical Journal*, 107:742–746, February 1994.

[31] Sbordone L. et al. ATLAS and SYNTHE under Linux. *Memorie della Societa Astronomica Italiana Supplementi*, 5:93, January 2004.

[32] Baschek B., Scholz M. and Wehrse R. The parameters R and Teff in stellar models and observations. *Astronomy & Astrophysics*, 246:374, June 1991.

[33] Smalley B. $T_{eff}$ and log $g$ determinations. *Memorie della Societa Astronomica Italiana Supplementi*, 8:130, January 2005.

[34] Matteucci F. *The Chemical Evolution of the Galaxy*. Springer, 1st edition, 2003.

[35] Shajn G. and Struve O. On the rotation of the stars. *Monthly Notices of the Royal Astronomical Society*, 89:222–239, January 1929.

[36] Heyrovsky D. Computing limb-darkening coefficients from stellar atmosphere models. *The Astrophysical Journal*, 656(1):483–492, February 2007.

[37] Nesvacil N. Stütz C. and Weiss W.W. ATLAS model atmospheres. In Ulisse Munari, editor, *GAIA Spectroscopy: Science and Technology*, volume 298 of *Astronomical Society of the Pacific Conference Series*, page 173, January 2003.

[38] Plez B. MARCS model atmospheres. *Physica Scripta Volume T*, 133:014003, December 2008.

[39] Gilmore G. et al. The Gaia-ESO public spectroscopic survey. *The Messenger*, 147:25–31, March 2012.

[40] Kupka F. et al. VAMDC as a resource for atomic and molecular data and the new release of VALD. *Baltic Astronomy*, 20:503–510, August 2011.

[41] Ryabchikova T., Fossati L. and Shulyak D. Improved fundamental parameters and LTE abundances of the CoRoT Solar-type pulsator HD 49933. *Astronomy & Astrophysics*, 506:203–211, May 2009.

[42] Fossati L. et al. The chemical abundance analysis of normal early A- and late B-type stars. *Astronomy & Astrophysics*, 503:945–962, September 2009.

[43] Pascual S. et al. MEGARA Data Reduction Pipeline. In *Highlights on Spanish Astrophysics X*, pages 227–227, March 2019.

[44] Brunsden E. et al. Spectroscopic pulsational frequency identification and mode determination of $\gamma$ Doradus star HD 12901. *Monthly Notices of the Royal Astronomical Society*, 427(3):2512–2522, December 2012.

[45] Bruntt H., De Cat P. and Aerts C. A spectroscopic study of southern (candidate) $\gamma$ Doradus stars. II. Detailed abundance analysis and fundamental parameters. *Astronomy & Astrophysics*, 478:487–496, February 2008.

[46] Gray R.O., Napier M.G. and Winkler L.I. The physical basis of luminosity classification in the late A-, F-, and early G-type stars. I. Precise spectral types for 372 stars. *The Astronomical Journal*, 121(4):2148–2158, April 2001.

[47] Watanabe Y. Kato K.-I. and Sadakane K. Atmospheric abundances of light elements in the F-type star Procyon. *Publications of the Astronomical Society of Japan*, 48:601–606, August 1996.

[48] J. Tomkin and D. L. Lambert. Carbon, nitrogen, and oxygen abundances in main-sequence stars. I - Procyon and the Hyades cluster stars 45 Tauri and HD 27561. *The Astrophysical Journal*, 223:937–948, August 1978.

[49] Kato K. and Sadakane K. A model atmosphere analysis of Procyon (alf CMi,F5 IV-V). *Astronomy & Astrophysics*, 113:135–141, September 1982.

[50] Steffen M. A model atmosphere analysis of the F5 IV-V subgiant Procyon. *Astronomy & Astrophysics Supplement Series*, 59:403–427, March 1985.

[51] Lane M.C. and Lester J.B. Atmospheric abundances of classical metallic-line A stars - The visual spectral region. *Astrophysical Journal Supplement Series*, 65:137–160, September 1987.

[52] Edvardsson B. et al. The chemical evolution of the galactic disk - Part one - Analysis and results. *Astronomy & Astrophysics*, 275:101, August 1993.

[53] Luck R.E. and Heiter U. Stars within 15 Parsecs: Abundances for a Northern Sample. *The Astronomical Journal*, 129(2):1063–1083, February 2005.

[54] Jofré P. et al. Gaia FGK benchmark stars: abundances of $\alpha$ and iron-peak elements. *Astronomy & Astrophysics*, 582:A81, October 2015.

[55] Liebert J. et al. The age and stellar parameters of the procyon binary system. *The Astrophysical Journal*, 769(1):7, Apr 2013.

[56] Santos A.R.G. et al. Surface rotation and photometric activity for kepler targets. i. m and k main-sequence stars. *The Astrophysical Journal Supplement Series*, 244(1):21, sep 2019.

[57] Cabrera Solana D., Bellot Rubio L.R. & del Toro Iniesta J. C. Sensitivity of spectral lines to temperature, velocity, and magnetic field. , 439(2):687–699, August 2005.

[58] Gray R.O., Graham P.W. and Hoyt S.R. The physical basis of luminosity classification in the late A-, F-, and early G-type stars. II. Basic parameters of program stars and the role of microturbulence. *The Astronomical Journal*, 121:2159, December 2007.

[59] Biémont E., Quinet P. and Ryabchikova T.A. Core-polarization effects in doubly ionized cerium (Ce III) for transitions of astrophysical interest. *Monthly Notices of the Royal Astronomical Society*, 336(4):1155–1160, November 2002.

[60] Holmberg J., Nordström B. and Andersen J. The Geneva-Copenhagen survey of the solar neighbourhood. *Astronomy  Astrophysics*, 501(3):941–947, May 2009.

[61] Cassatella A. On the Analysis of Blended Spectra. , 48:281, April 1976.

# A Appendices

## A.1 SIMBAD Parameter Values for Standard Stars

| Target | $T_{eff}(K)$ | log $g$ (dex) | [Fe/H] | $v_{mic}$ (kms$^{-1}$) | Reference |
|---|---|---|---|---|---|
| HD 22879 | 5858 | 4.37 | -0.85 | 0.68 | 2018 A&A 615A 76S |
| | 5858 | 4.37 | -0.85 | 0.68 | 2018 A&A 615A 76S |
| | 5920 | 4.33 | -0.84 | 1.20 | 2003 A&A 410 527B |
| | 5913 | 4.53 | -0.73 | 1.21 | 2015 A&A 580A 24D |
| | 5884 | 4.52 | -0.82 | 1.20 | 2011 A&A 526A 99S |
| | 5859 | 4.29 | -0.86 | 1.20 | 2014 A&A 568A 25N |
| | 5857 | 4.46 | -0.83 | 1.23 | 2008 A&A 487 373S |
| | 5827 | 4.33 | -0.83 | 0.46 | 2003 A&A 404 187G |
| | 5808 | 4.40 | -0.91 | 0.79 | 2007 A&A 465 271R |
| | 5800 | 4.29 | -0.84 | 1.00 | 2015 ApJ 808 148S |
| | 5778 | 4.25 | -0.84 | 1.06 | 2006 A&A 449 127Z |
| | 5775 | 4.26 | -0.83 | 1.10 | 2006 A&A 451 1065G |
| | 5759 | 4.25 | -0.85 | 1.30 | 2010 A&A 511L 10N |
| | 5970 | 4.50 | -0.81 | 4.52 | 2016 A&A 586A 49B |
| | 5884 | 4.52 | -0.81 | 1.20 | 2014 A&A 562A 92D |
| | 5970 | 4.50 | -0.81 | 4.52 | 2015 A&A 577A 9B |
| | 5970 | 4.52 | -0.81 | 1.27 | 2014 A&A 562A 71B |
| | 5949 | 4.68 | -0.79 | 1.63 | 2013 A&A 555A 150T |
| | 5910 | 4.30 | -0.83 | 1.30 | 2013 ApJ 764 78R |
| | 5891 | 4.31 | -0.82 | 1.58 | 2012 ApJ 756 46R |
| | 5884 | 4.52 | -0.82 | 1.20 | 2012 A&A 545A 32A |
| HD 49933 | 6657 | 4.10 | -0.40 | 1.66 | 2016 A&A 589A 115S |
| | 6700 | 4.25 | -0.34 | 1.65 | 2006 A&A 448 341G |
| | 6735 | 4.26 | -0.37 | 1.84 | 2006 A&A 448 341G |
| | 6467 | 4.27 | -0.37 | 2.53 | 2006 A&A 448 341G |
| | 6539 | 4.41 | -0.45 | 2.12 | 2006 A&A 448 341G |
| | 6538 | 4.38 | -0.47 | 2.33 | 2006 A&A 448 341G |
| | 6600 | 4.15 | -0.47 | 1.70 | 2015 ApJ 808 148S |
| | 6522 | 4.00 | -0.49 | 1.96 | 2005 PASJ 57 27T |
| | 6620 | 4.19 | -0.40 | 1.88 | 2013 ApJ 764 78R |
| HD 61421 | 6850 | 4.55 | -0.04 | 2.40 | 2003 AJ 126 2015H |
| *(Procyon)* | 6850 | 4.45 | -0.04 | 2.40 | 2006 AJ 131 3069L |
| | 6850 | 4.45 | -0.04 | 2.40 | 2005 AJ 129 1063L |
| | 6677 | 4.08 | +0.03 | 1.72 | 2004 A&A 420 183A |
| | 6660 | 4.05 | -0.04 | 1.70 | 2013 MNRAS 428 3164D |
| | 6650 | 4.05 | +0.03 | 2.20 | 2010 A&A 523A 71G |
| | 6632 | 4.02 | +0.01 | 1.90 | 2004 A&A 425 187T |
| | 6612 | 4.00 | -0.02 | 1.97 | 2005 PASJ 57 27T |
| | 6593 | 3.90 | +0.02 | 1.80 | 2010 MNRAS 403 1368G |
| | 6560 | 4.00 | -0.02 | 1.20 | 2000 ApJ 530 939C |

Temperature, gravity, metallicity and microturbulence results for standards taken from the SIMBAD archive.

| Target | $T_{eff}(K)$ | log $g$ (dex) | [Fe/H] | $v_{mic}\,(kms^{-1})$ | Reference |
|---|---|---|---|---|---|
| HD 61421 | 6545 | 3.99 | +0.01 | 1.80 | 2014 A&A 564A 133J |
| *(Procyon)* | 6510 | 3.96 | -0.03 | 1.83 | 2003 A&A 407 691K |
| | 6510 | 3.96 | -0.03 | 1.80 | 2008 A&A 492 823B |
| | 6485 | 3.89 | +0.01 | 1.69 | 2010 MNRAS 405 1907B |
| | 6554 | 3.99 | -0.04 | 2.10 | 2016 A&A 587A 2B |
| | 6612 | 4.00 | -0.02 | 1.97 | 2007 PASJ 59 335T |

Temperature, gravity, metallicity and microturbulence results continued.

| Target | $v\sin i$ ($\mathrm{kms}^{-1}$) | Reference |
|---|---|---|
| HD 22879 | 0.00 | 2018 A&A 615A 76S |
| | 1.30 | 2014 MNRAS 444 3517M |
| | 2.12 | 2010 A&A 520A 79M |
| HD 49933 | 5.0 | 2005 PASJ 57 13T |
| | 10.14 | 2014 A&A 570A 80T |
| | 14.0 | 2004 A&A 425 683B |
| | 10.3 | 2006 A&A 448 341G |
| | 10.0 | 2006 A&A 448 341G |
| | 12.3 | 2016 ApJS 225 32B |
| HD 61421 | 5.39 | 2010 A&A 520A 79M |
| *(Procyon)* | 3.90 | 2009 A&A 493 1099S |
| | 3.00 | 2005 PASJ 57 13T |

Rotation results for standards taken from the SIMBAD archive.